LASER ABSORPTION MEASUREMENTS OF CO AND H2O FROM DIMETHYL CARBONATE COMBUSTION BEHIND REFLECTED SHOCK WAVES FOR SAFER LI-ION BATTERY APPLICATIONS

A Thesis

by

TATYANA MABEL ATHERLEY O'MEALLY

Submitted to the Office of Graduate and Professional Studies of
Texas A&M University
in partial fulfillment of the requirements for the degree of

MASTER OF SCIENCE

Chair of Committee,	Eric L. Petersen
Co-Chair of Committee,	Olivier Mathieu
Committee Members,	Chad Mashuga
Head of Department,	Bryan P. Rasmussen

May 2021

Major Subject: Mechanical Engineering

ABSTRACT

Dimethyl Carbonate (DMC) is a carbonate ester that can be produced in environment-friendly ways, from sources such as biomass or methanol and CO_2. DMC can be used as a diesel fuel additive and is also one of the main components of the flammable electrolyte used in Li-ion batteries. Studying the combustion chemistry of DMC can therefore improve the use of biofuels and help in developing safer Li-ion batteries. The combustion chemistry of DMC has been investigated in a limited number of studies, and a few detailed kinetics models have been proposed in literature. The aim of this study was to complement the scarce data available for DMC combustion in the literature and to improve a detailed kinetic model.

Shock tubes were used to measure time histories of CO and H_2O using tunable laser absorption techniques for the first time for DMC. Characteristic reaction times were also measured through OH* emission. Shock-tube spectroscopic measurements were performed under dilute conditions, at three equivalence ratios (fuel-lean, stoichiometric, and fuel-rich) between 1260 and 1660 K near 1.3±0.2 atm, and under pyrolysis conditions (98%+) ranging from 1230 to 2500 K near 1.3±0.2 atm. The model comparison and validation were further broadened using new laminar flame speed data collected in CNRS ICARE, France. Flame speeds at 318 K, 363 K and 464 K measured for equivalence ratios of 0.7-1.5 in a spherical vessel around atmospheric pressure were used to further extend the range of conditions investigated. Detailed kinetics models from the literature were compared to the data, and it was found that none can accurately predict the new data over

the entire range of conditions investigated. A numerical analysis was performed, and updates to the most accurate model allowed for a significant improvement of the predictions for DMC combustion.

ACKNOWLEDGMENTS

I will perpetually be grateful to my advisor, Dr. Eric L Petersen, for the opportunity to join his lab and work in various exciting projects, for the unconditional support and guidance throughout the pursuit of my degree. Thank you for allowing me to learn from your high-quality instructions, lecturing skills, and determination to continue learning (about gas dynamics and combustion science). I would also like to thank my co-advisor Dr. Mathieu and committee member Dr. Mashuga, for their guidance and support throughout my master's degree. Special thanks to Laura Pinzon for making the initial referral to the Petersen Research Group.

Immense gratitude goes to my supervisor, mentor and friend, Dr. Olivier Mathieu, for his countless teachings in both research work and life. Thank you for all the shock tube operational teachings, Chemkin teachings, data post processing teachings and unconditional support.

I would also like to thank Clayton Mulvihill and Sulaiman Alturaifi for their work on the laser diagnostics section and their help and patience in optics and post processing assistance. My sincerest gratitude goes to Dr. Nabiha Chaumeix and her team, from ICARE, CNRS Orléans, France, who shared her research work with us.

Finally, thanks to my friends, lab colleagues, department faculty, staff and peers for the warmth and help. Lastly, my family and support system, thank you for your light that helps me grow.

CONTRIBUTORS AND FUNDING SOURCES

Contributors

This work was supervised by a thesis committee consisting of Professors Eric L. Petersen (advisor) and Olivier Mathieu (co-advisor) of the Department of Mechanical Engineering and Professor Chad Mashuga of the Department of Chemical Engineering.

The laser diagnostics used in this work have been but in place by Dr. Clayton Mulvihil and Sulaiman Alturaifi, Ph.D. candidate of the Department of Mechanical Engineering and members of the Petersen Research Group.

The data presented for Section 3.4 were provided by Professor Dr. Chaumeix, from CNRS, ICARE, Orléans, France. The analyses depicted in Section 3.4 were conducted together with Dr. Chaumeix et al. and were originally published in 2020. Funding for the flame speed experiments came from the “Conseil Régional du Centre-Val de Loire”, France.

All other work conducted for the thesis was completed by the student.

Funding Sources

This study was made possible in part thanks to the J. Mike ’66 Department of Mechanical Engineering from Texas A&M University under the Summer 2019 Graduate Research Grant and additional instrumentation and funding were provided from the Dr. Petersen Research Group and the TEES Turbomachinery Laboratory.

NOMENCLATURE

HPST	High pressure shock tube
LPST	Low pressure shock tube
ST	Shock Tube
DMC	Dimethyl-carbonate
CO	Carbon Monoxide
H_2O	Water
LIB	Lithium-ion battery
EV	Electric vehicle
PHEV	Plug-in hybrid electric vehicle
φ	Equivalence Ratio
k_1	Rate Coefficient
τ_{ign}	Ignition Delay Time
MT	Mixing Tank
P	Static Pressure
t	Time
T	Static Temperature
RCM	Rapid Compression Machine
ROP	Rate-of-Production
RMS	Root mean square roughness
I	Transmitted intensity

I_0	Incident intensity
k_v	Absorption coefficient ($cm^{-1}atm^{-1}$)
P_{abs}	Partial pressure of water
L	Path length
TDL	Tunable diode laser
$S(T)$	Linestrength
$\phi(\bar{v}\text{-}\bar{v}_0)$	Lineshape
ϑ_{ki}	Stoichiometric coefficient for the reactions
q_i	Rate of progress of the I gas-phase reaction
Subscripts	
1	Initial condition of the driven section of the shock tube at t = 0
2	Condition behind the incident shock wave
3	Condition in the driver section behind the contact surface and the expansion wave
4	Initial condition of the driver section at t = 0
5	Condition behind the reflected shock wave in the driven section

TABLE OF CONTENTS

Page

LIST OF FIGURES

Page

LIST OF TABLES

Page

1. INTRODUCTION AND LITERATURE REVIEW*

1.1. Motivation

Dimethyl Carbonate ($CH_3OCOOCH_3$, DMC) is an interesting molecule that can help mitigate greenhouse emissions from transportation in several ways. First, DMC is a promising biofuel that can be directly synthesized from CO_2 and methanol [1] and can be used as an additive in diesel fuel. Besides its environmentally friendly production mechanism, its usage in internal combustion engines leads to a reduction in soot emissions without penalty on the engine's thermal efficiency or NOx emissions [2, 3].

Secondly, DMC is a major component of Li-ion battery (LIB) electrolytes, a flammable mixture of linear and cyclic carbonates [4] that allows Lithium salt ions to flow between the cathode and the anode. The flammability of the electrolyte has led to many fire incidents, ranging from cell phones to airplanes, with many electric vehicles catching fire after a traffic accident of during the charging process. These fire incidents are due to flaws in the design or fabrication processes or physical damages of the LIB [4]. With the rapidly growing number of electric vehicles on the roads, exposing large LIB to mechanical damage, and the rising use of mobile/portable devices, it is important to understand the combustion chemistry of LIB electrolyte components, to work towards

---

* Parts of this section are reprinted with permission from "Laminar flame speed and shock-tube multi-species laser absorption measurements of Dimethyl Carbonate oxidation and pyrolysis near 1 atm" by Atherley, T., de Persis, S., Chaumeix, N., Fernandes, Y., Bry, A., Comandini, A., Mathieu, O., Alturaifi, S., Mulvihill, C. R., Petersen, E. L., 2021, *Proceedings of the Combustion Institute*, Vol. 38, pp. 977-985, Copyright 2020 The Combustion Institute. Published by Elservier Inc. https://doi.org/10.1016/j.proci.2020.06.333

reducing their flammability. To the best of the author's knowledge, there are only a few articles investigating the fundamental combustion chemistry of the carbonate solvents used in Li-ion batteries [5, 6].

The present study aims to do so by experimentally investigating DMC combustion chemistry, with an assortment of important combustion parameters measurements, such as ignition delay time and laminar flame speed, and more fundamental experiments such as laser-absorption measurements of CO and H_2O using shock tubes. Detailed kinetics mechanisms from Glaude et al. [7], Hu et al. [8], Sun et al. [9], and Alexandrino et al. [10] were compared to the data to assess their accuracy. Provided in this thesis is the description of the experimental facilities, followed by the presentation of the experimental results and the comparison of the kinetics models. Finally, a numerical analysis was performed, leading to model improvements and recommendations for future work.

1.2. Background

1.2.1. Lithium-Ion Battery Research

Batteries are key to a more efficient use of energy and are essential in the pursuit to electrify road transportation. Lithium-Ion Batteries (LIBs) have dominated the portable electronics market and are thought of as the solution for electric vehicles (Plug-in hybrid electric vehicle (PHEV) or EVs) and for renewable energy storage. LIBs remain a global leading technology thanks to their high energy density and other advantageous properties such as low self-discharge, and lack of memory effect. Literature shows that LIB

technology still falls behind when it comes to considering its use in mainstream EV adoption, in which parameters are often disregarded such as safety risks or concerns. As we transition toward electric mobility, it is imperative to do so in a strategic manner, since the electricity used to power or charge this application comes from the power grid encompassing renewables sources, carbon-free and fossil fuel power plants.

LIBs operate by moving lithium salt ions through an electrolyte and through a separator from the anode to the cathode during the discharge, and the process reverses during charging, as can be observed in Figure 1.

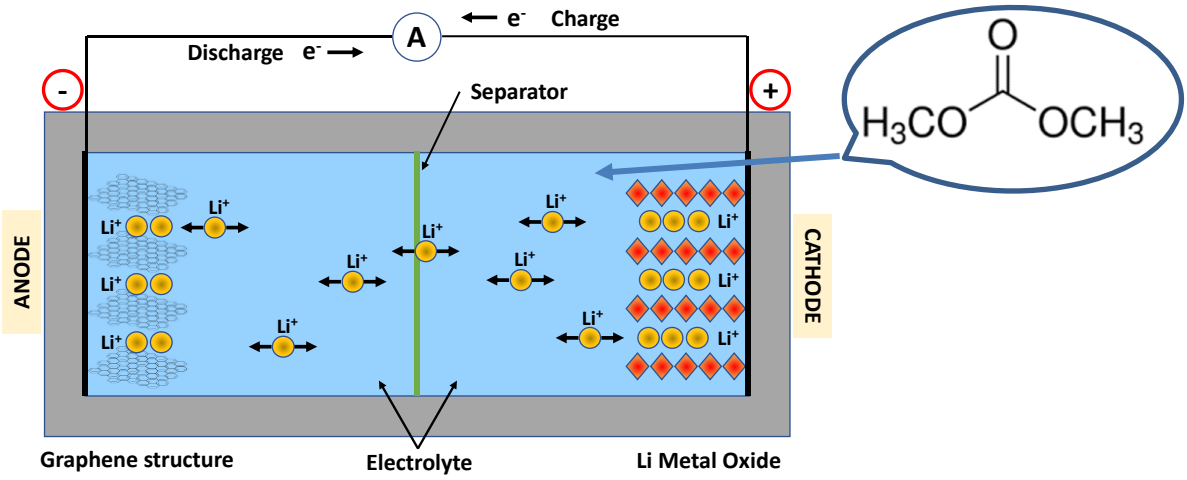

Figure 1. Schematic of common Li-ion battery operating principle.

The electrolyte component of LIBs is a highly flammable organic solvent material known for causing issue at all phases of the LIB's life: from factory production, during usage, and when disposing/recycling the used batteries [11, 12]. This organic solvent is composed of a mixture of linear (dimethyl-carbonate (DMC), diethyl-carbonate (DEC), ethyl-methyl-carbonate (EMC)) and cyclic carbonates (propylene carbonate (PC),

ethylene carbonate (EC), to name a few). Literature [13, 14] claims this type of mixture is beneficial to LIBs due to its low viscosity and high volatility, which enhances the electrode's wettability. The high flammability characteristics of the electrolyte makes this a possible fire hazard during its usage in case of any damage or flaw during its design or fabrication processes.

A LIB fire is primarily due to an internal short circuit due to three main types of abuses: mechanical, electrical, and thermal. Noting that these abuses can be linked; a mechanical abuse inducing an electrical abuse, which then leads to a thermal abuse presented in forms of thermal runaway, and potential fire or explosion, as shown in Figure 2.

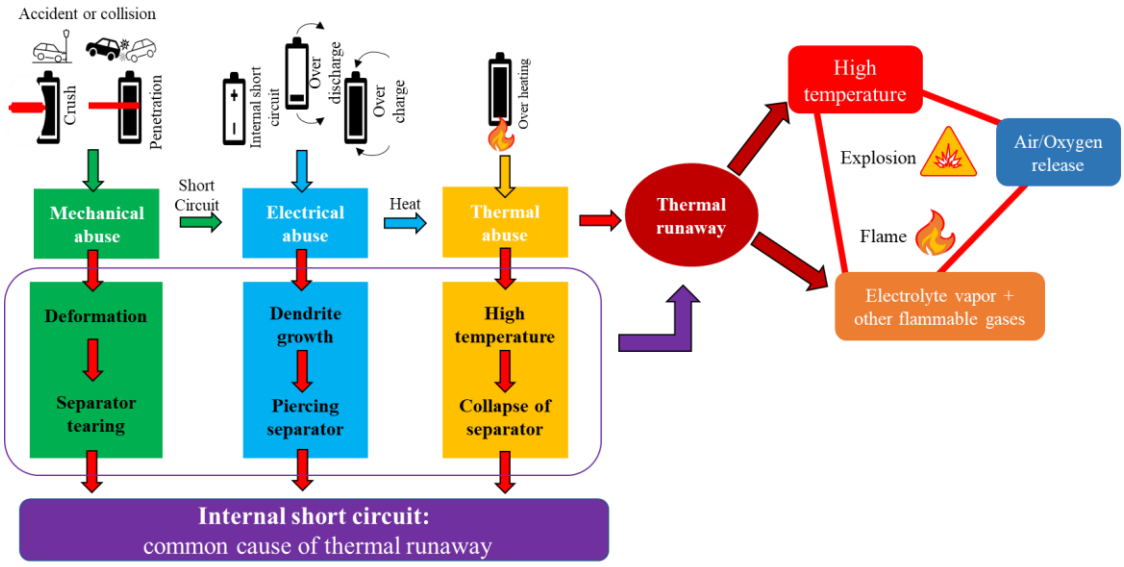

Figure 2. Schematic of the cause of LIB fire accidents [14].

1.2.2. EV mainstream adoption and LIB safety concerns

It is evident that climate change and the decline of prices have certainly catalyzed the movement towards renewable ‘green’ energy. This vision has also been adopted by automakers, that project that EVs will be the future. In EVs, the car battery pack is the single most expensive component, therefore its cost has a direct impact on the cost of the car. The average price of LIB packs dropped 89% in a 10-year span (to $137/kWh in 2020 and is now down to $100/kWh) [15]. The results of these efforts can be presently noticed as EVs become more affordable and technology continues to improve, hence promoting its mass adoption. Today, EVs are near the tipping point for mainstream adoption, EVs are expected to account for more than 38% of total sales in the US by 2025 and 18% of the global market [16].

Recently, we have been overwhelmed by the large amount of news related to the shift towards EV adoption. Carmakers are being forced to invest in new technologies and redesign their business model due to recent emissions regulations/bans and future zero emission targets. Policies are already taking place in Europe and China, and soon in California.

As the world shifts towards a ‘green’ mentality, we cannot disregard the importance of environmental and sustainable objectives in the adoption of new technologies. Examples of such efforts include 17 countries announcing 100% zero emission vehicle targets or the phase-out of IC engine vehicles through 2050 [17]. The fall in EV batteries can be attributed to the research conducted to improve all three key components of LIBs cells: cathodes, anodes and electrolytes.

Current research conducted for LIBs is steered in the direction of improving the battery design and thermal management. Thermal management research seems more focused on the impact for better performance than on the combustible characteristics. Furthermore, when it comes to fire-related studies, the approach is often undeveloped, without discussing combustion kinetics mechanisms. Safety, a variable that has been historically difficult to assess, becomes an important parameter when considering high volumes of EVs on the road and their fire hazard potential.

1.2.2.1. Fire incident Reports

Concerns and criticism regarding EV safety are now surfacing, due to the increase in incident reports related to LIB fires in EVs. Over the years, multiple carmakers have had to recall their EV model due to fire incidents or faulty batteries.

Hyundai and GM are currently debating whether the carmaker or the battery maker is responsible for their battery incidents that cause significant recalls. On February 2021, Hyundai, the fourth largest EV manufacturer in the world, reported it will recall 76,000 EVs globally due to potential fire hazards. This event represents the most expensive EV-related recall. In 2019, GM recalled 69,000 Chevy Bolts due to similar incidents. Other companies that have recalled their EV models due to battery fires include Audi (1,600 E-tron model), BMW (27,000 PHEVs), Ford, (27,000 Kuga PHEV), all the above, occurred in 2019.

It is expected for the increase of EVs on the road to have a direct impact/relation with the number of EV-related collisions. An increase in EV collisions, increases the

probability of damage of the battery pack/LIB damage, which can lead to a fire hazard. In EVs, larger and larger the battery cell packs are being used, and, in this case, it can be said that safety is being compromised over performance, since a larger battery pack means more exposure to LIB damage hence more susceptible to fire risk.

The National Highway Traffic Safety Administration stated that cell packs of affected vehicles have the potential to smoke and ignite internally, which could spread [18]. The issue can be further extended based on reports of unpreparedness of the fire departments and first responders in cities where EVs have become available.

Other examples of LIB fire incidents that resulted in a product recall or ban include: Sony's 2006 fire hazard laptop recall of more than 10 million laptops battery packs [19], Samsung's 2016 Galaxy Note 7 phones confirmed fire events [20], flight bans on specific devices, among others.

1.2.3. Mechanisms in Literature

The incidents mentioned above together with the increased interest and search for more efficient means of energy, have fueled research in LIBs such as thermal decomposition, but not in fundamental combustion chemistry, to the author's best knowledge. For this reason, the present study aims to highlight the importance of fundamental chemical kinetics studies for better combustion chemistry understanding that enables possibilities of finding fire suppressants and enhance predictions through model validation.

The mechanisms for DMC combustion in the literature are limited. Table 1 summarizes the mechanisms found and applied for model comparison with experimental data further on.

Table 1 Dimethyl-carbonate mechanisms in literature.

Mechanism	Year	No. of Species	No. of Reactions
Glaude et al. [7]	2005	103	442
Hu et al. [8]	2015	275	1584
Sun et al. [9]	2016	257	1563
Alexandrino et al. [10]	2018	497	2737

In 2005, motivated by its high oxygen content and low soot formation characteristics, Glaude et al. [7] developed the first chemical kinetic model of DMC using an opposed-flow diffusion flame. The experimental results were used to obtain the new reaction rate constants included in what this study refers to as the 'Glaude et al.' mechanism. Subsequently, in 2015 Hu et al. [8] performed the first ignition delay time measurements of DMC at high temperatures using a shock tube and developed a modified chemical kinetic model, the 'Hu et al.' model. The following year, Sun et al. [9] further complemented the DMC pyrolysis and oxidation data in the literature through their detailed chemical kinetics model, further assessed with measurements using flow reactor and low-pressure premixed flames. Lastly, Alexandrino et al. [10] developed the last model that will be used in this study for model comparison. The 'Alexandrino et al.' model is based after ignition delay time measurements of DMC using shock tubes and RMC facilities. This final model is composed of the AramcoMech 2.0 used as the base

mechanism and the modified DMC submechanism. The model of Alexandrino et al. was used in this study for *the* numerical analysis of the experimental results, as will be discussed in the following section.

1.3. Scope and Organization of this Thesis

The present study aims to highlight the need for better combustion understanding of the components used in LIBs. Upon establishing that the electrolyte is a highly flammable component present in the battery, DMC was selected due to its high-level usage in LIBs, as well as in biofuel and additive capabilities. The study was accomplished by fundamentally studying the combustion of Dimethyl Carbonate (DMC) using two shock-tube facilities. CO and H_2O measurements from DMC combustion using laser absorption measurement techniques in shock tubes were obtained for the first time. These shock-tube experiments were performed for DMC pyrolysis and oxidation at three equivalence ratios. Experiments were then compared to models from the literature. After a numerical analysis, a tentative model was proposed in this study.

Section 2 describes the experimental facility, the optical setup for species emissions diagnostics, delay time measurement methods, and software tools for numerical analysis. Section 3 presents the results including the experimental profiles plotted with models in the literature and the tentative model proposed in This Study. Section 4 summarizes this work and includes future work suggestions in Conclusions and Recommendation. The Appendix sections present the data for all shock-tube experiments conducted in this study, followed by additional supplemental material relevant to this study.

2. EXPERIMENTAL METHODOLOGY*

Shock tubes are commonly used for fundamental combustion chemistry studies and, were the primary experimental apparatus used for this research work. Figure 3 shows a schematic representation of the main section composing a shock tube.

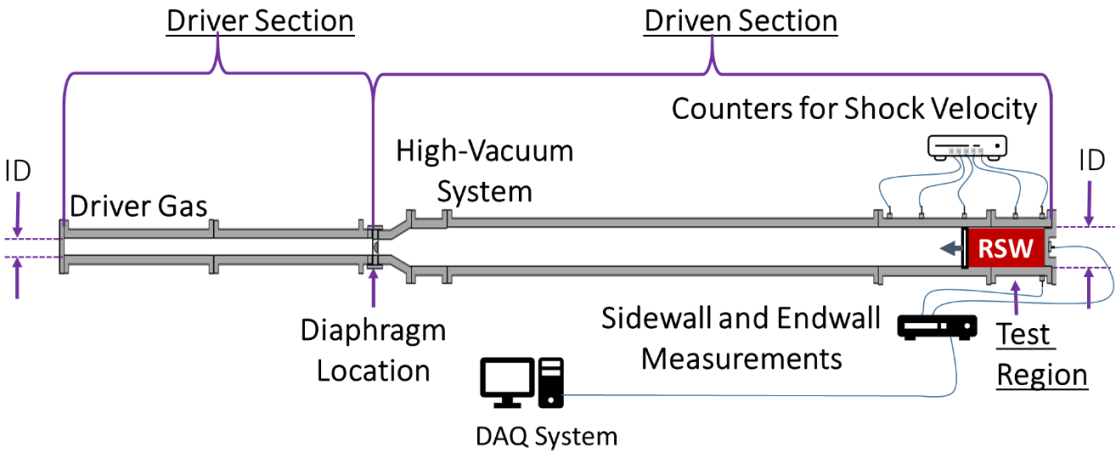

Figure 3. Schematic displaying main sections of a stainless-steel shock tube.

2.1. Shock Tubes

Two shock tubes were used in this study, further referred to as the CO/OH* and H_2O tubes. The CO/OH* tube is 6.1-m long with a 4-m, 10.8-cm square driven section. The H_2O tube has a 6.78-m-long driven section (16.2-cm ID) and a 3-m-long driver section. Both tubes are made of stainless-steel and have a single-diaphragm arrangement. Several

* Parts of this section are reprinted with permission from "Laminar flame speed and shock-tube multi-species laser absorption measurements of Dimethyl Carbonate oxidation and pyrolysis near 1 atm" by Atherley, T., de Persis, S., Chaumeix, N., Fernandes, Y., Bry, A., Comandini, A., Mathieu, O., Alturaifi, S., Mulvihill, C. R., Petersen, E. L., 2021, *Proceedings of the Combustion Institute*, Vol. 38, pp. 977-985, Copyright 2020 The Combustion Institute. Published by Elservier Inc. https://doi.org/10.1016/j.proci.2020.06.333

piezoelectric pressure transducers (PCB P113A) are located along the driven sections to determine the incident shock wave velocity. All signals were recorded using a 14-bit GageScope digital oscilloscope with sampling rates per channel of 1 MHz or above. A linear fit was used to extrapolate this velocity to the endwall location, which coupled with the one-dimensional shock relations and initial conditions, was used to determine the reflected-shock temperature (T_5) and pressure (P_5). These reflected-shock conditions have an estimated uncertainty of ~1.0% [21]. Table 2 summarizes the dimensions of the shock tubes used.

Table 2 Shock-Tube facilities dimensions.

Shock Tube	**CO/OH***	**H_2O**
Driver Section length (m)	2	3
Driver Section ID (cm)	7.6	7.62
Driven Section length (m)	4	6.78
Driven Section ID (cm)	10.8	16.2

Before each experiment, the driven sections of the tubes were vacuumed to ~10^{-5} Torr using a combination of roughing and turbomolecular pumps. All test mixtures were prepared manometrically in stainless-steel tanks using 0-10 Torr, 0-1000 Torr, and 0-13,000 Torr pressure gauges. The DMC was provided by Sigma-Aldrich® (≥99%), while O_2, Ar, and He were supplied by Praxair®, 99.999% purity. DMC was introduced in the mixing tank via a vial, after being de-gassed at least three times. Three equivalence ratios (ϕ), 0.5, 1.0, and 2.0, were studied between 1260 and 1660 K at 1.3±0.1 atm, for mixtures diluted at 99.25%. Pyrolysis of DMC was investigated as well, ranging from 1230 to 1560 K near 1.6±0.06 atm with a dilution set to 99.75% for the CO measurement and 1980

to 2500 K near 1.1±0.09 atm with 98% dilution for H_2O. The dilution levels used for this study were determined based on the allowable detection levels for proper and accurate laser absorption measurements. A high dilution level is also desirable as it mitigates the temperature changes induced by the mixture's reactivity (more on this below). Note that 20% He was added (balance Ar) in the mixtures for CO measurements, due to possible vibrational relaxation effects [22]. A summary of all the experimental conditions investigated, along with the exact composition of the mixtures, can be seen in Table 3.

Table 3 Shock-tube conditions investigated for oxidation and pyrolysis of DMC.

Species Measurement	**Mixture composition**			**Equiv. Ratio (ϕ)**	**P_5 (atm)**	**T_5 (K)**
Shock Tube	**% DMC**	**% O_2**	**%Ar**			
CO/OH*	0.1071	0.6429	79.25 (20% He added)	0.5	1.28±0.05	1316-1474
	0.1875	0.5625		1.0	1.33±0.08	1323-1573
	0.3	0.45		2.0	1.25±0.10	1307-1642
	0.25	0	79.75 (20% He)	∞	1.57±0.06	1232-1556
H_2O	0.1071	0.6429	99.25	0.5	1.41±0.06	1304-1546
	0.1875	0.5625	99.25	1.0	1.32±0.09	1260-1573
	0.3	0.45	99.25	2.0	1.37±0.07	1354-1658
	2.01	0	97.99	∞	1.09±0.09	1980-2499

2.2. Laser Diagnostics

The fundamental relation of the spectroscopic diagnostics used herein is the Beer-Lambert relation, $I/I_0 = \exp(-k_v P X_{abs} L)$, where I and I_0 are the transmitted and incident laser intensities, respectively; k_v the absorption coefficient ($cm^{-1}atm^{-1}$), P the pressure (atm), X_{abs} the species mole fraction, and L the path length (cm). The absorption coefficient, k_v is the product of the linestrength (obtained from HITRAN 2004 [23]) and

the lineshape (calculated using the Ar-broadening parameters from Ren et al. [24] for CO and Nagali et al. [25] for H_2O). Estimated concentration level uncertainties are ±5.6% for H_2O and ±3.8% for CO.

2.2.1. CO Laser Diagnostic

The CO diagnostic was assembled using a quantum cascade laser with a 1.5-MHz linewidth permitting access to the R(12) transition in the 1←0 band of CO at 4566.17 nm. A schematic representation can be seen in Figure 4. Throughout the experiments, the laser was centered at this CO transition line using a separate CO/Ar absorption cell. Laser intensities were recorded using InSb detectors equipped with bandpass filters (centered at 4500 nm, full width of 500 nm) allowing a decrease in the broadband emission levels entering the detectors to <0.3% of the absorbed signal. Minor CO_2 absorption occurs at this wavelength, and the procedure described by Mulvihill et al. [26] was utilized to correct the CO time-histories. For further details on the CO diagnostics, see [26] and references therein.

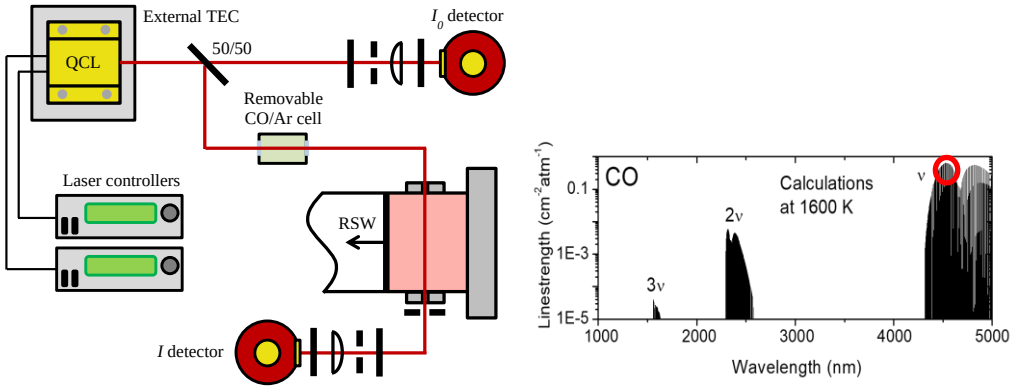

Figure 4. CO laser diagnostics and optics setup [26].

2.2.2. H_2O Laser Diagnostic

The H_2O diagnostic, depicted in Figure 5, uses a Toptica Photonics DL100L tunable diode laser set to 1388.140 nm, monitored using a Burleigh WA-1000 wavemeter. The incident and transmitted laser intensities were measured using two Newport 2317NF InGaAs detectors, fitted with a bandpass filter centered at 1388 nm with a full width, half maximum of 10 nm. The laser beam path was purged with N_2 to reduce the beam attenuation due to the air humidity. More details on the H_2O diagnostic can be found in Mathieu et al. [27]. Note that an emission experiment with the laser turned off was performed, and no broadband emission was captured by the detector, even for the very high temperatures investigated for the pyrolysis case.

The change in k_v with temperature was considered for each experiment, using the temperature change predicted by the Alexandrino et al. mechanism [10]. Further details on this correction method are described in recent work by the authors [26].

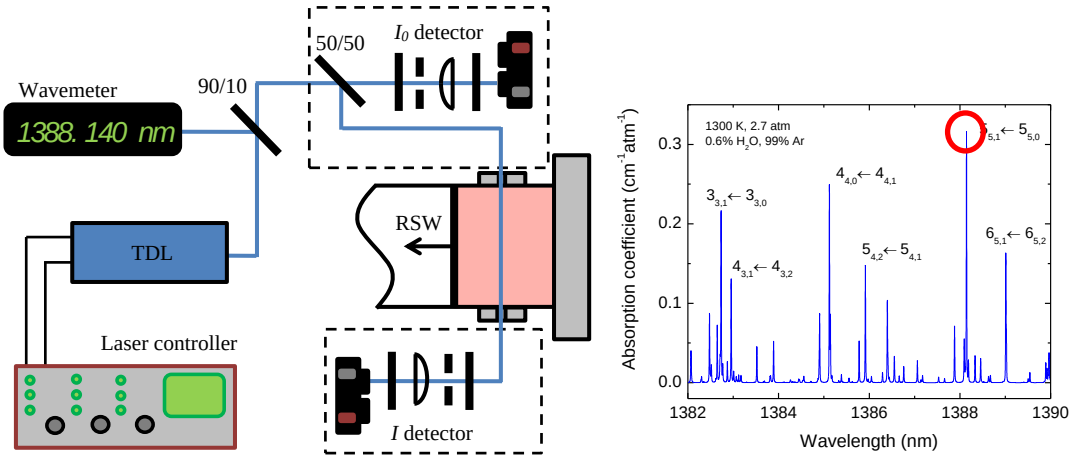

Figure 5. Water laser diagnostics setup and Absorption coefficient versus wavelength plot [26].

2.3. OH* Diagnostic

A Hamamatsu 1P21 photomultiplier tube with a 307±10 nm bandpass filter was used to capture the emission from the $A^2\Sigma^+ \rightarrow X^2\Pi$ transition of OH. The characteristic reaction time used herein is the time to peak OH* (τ_{peak}) and is defined as the time where the maximum level of the OH* signal was observed. Note that the test time is not long enough for the low-temperature cases to observe this peak and taking the time at the peak allows for characterization at higher temperatures, hence allowing a wider range of conditions. A typical τ_{peak} measurement is visible in Fig. 6. The estimated 15% uncertainties for τ_{peak} comes mainly from the uncertainties in T_5.

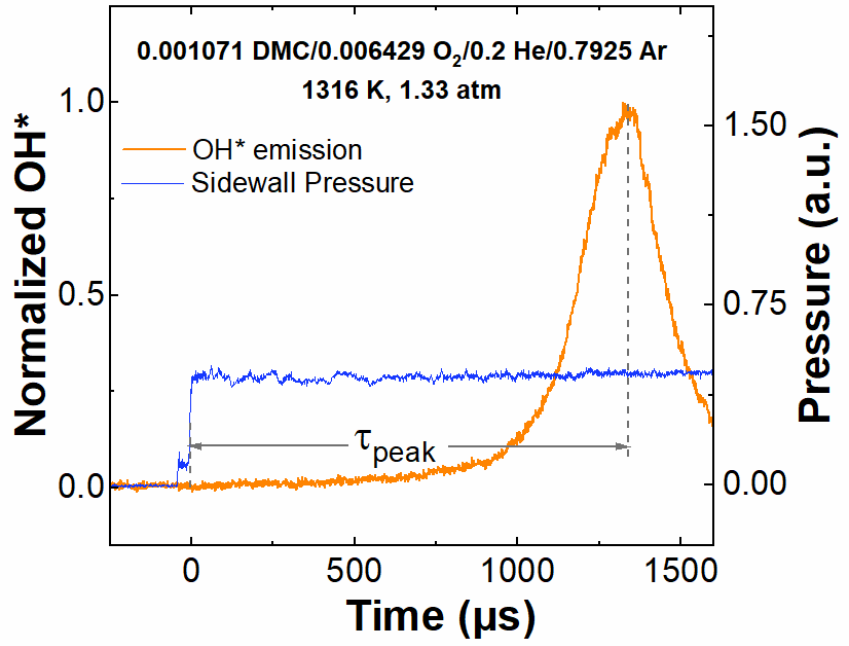

Figure 6. OH* emission and sidewall pressure emission signals recorded in this study with t_{peak} definition.

3. EXPERIMENTAL RESULTS AND MODEL COMPARISON*

It has been previously noted that trace hydrocarbon impurities, which are difficult to fully remove from shock-tube experiments, can noticeably accelerate the ignition of highly dilute hydrogen-based mixtures by decomposing into radicals such as H atoms and accelerating the growth of the radical pool [28]. Recently, a comprehensive study on the effects of impurity during shock tube experiments was conducted by Mulvihill et al. [29]. These authors concluded that hydrocarbons were not subject to impurities like hydrogen is. However, these authors did not perform their analysis with DMC, which is not a "traditional" hydrocarbon in combustion such as methane, propane or iso-octane, all used in the Mulvihill et al. study. Since DMC is much more reactive than methane or the other hydrocarbon investigated, the effect of impurities was investigated for the shock-tube results of the present study, using the work of Urzay et al. [28] to define the level of H impurities under the temperatures investigated herein. Calculations with and without H impurities in the mixtures were performed with the model of Alexandrino et al., the most accurate model from the literature (more on this below), and no difference in the results between the two mixtures was observed. Provided below are the results of the CO and

* Parts of this section are reprinted with permission from "Laminar flame speed and shock-tube multi-species laser absorption measurements of Dimethyl Carbonate oxidation and pyrolysis near 1 atm" by Atherley, T., de Persis, S., Chaumeix, N., Fernandes, Y., Bry, A., Comandini, A., Mathieu, O., Alturaifi, S., Mulvihill, C. R., Petersen, E. L., 2021, *Proceedings of the Combustion Institute*, Vol. 38, pp. 977-985, Copyright 2020 The Combustion Institute. Published by Elservier Inc. https://doi.org/10.1016/j.proci.2020.06.333

H_2O time history measurements, followed by the results of the characteristic time and laminar flame speed tests.

3.1. Carbon Monoxide (CO) Laser Absorption Measurements

CO time histories were obtained at low-, mid-, and high- temperatures for DMC oxidation and pyrolysis. These measurements were later compared with model predictions. The following subsections aim to find means of understanding the thermal breakdown of species such as DMC and other that play an important role in that they can impact both safety and functionality/proper operation.

3.1.1. CO measurements for DMC oxidation

The CO time histories for DMC oxidation were taken at three different equivalence ratios, fuel-lean (ϕ = 0.5), stoichiometric (ϕ = 1.0) and fuel-rich (ϕ = 2.0) and were later categorized by low-, mid-, and high- temperature ranges. The laser measurements show how the carbon monoxide formation starts very rapidly and reach a peak for all cases except for the low temperature conditions at ϕ = 1.0 and 2.0, where the CO formation does not reach a peak as it occurs after the shock-tube test-time. Overall, it was observed that the timing or delay for reaching this peak, decreases as the temperature increases, as can be observed in Figure 7.

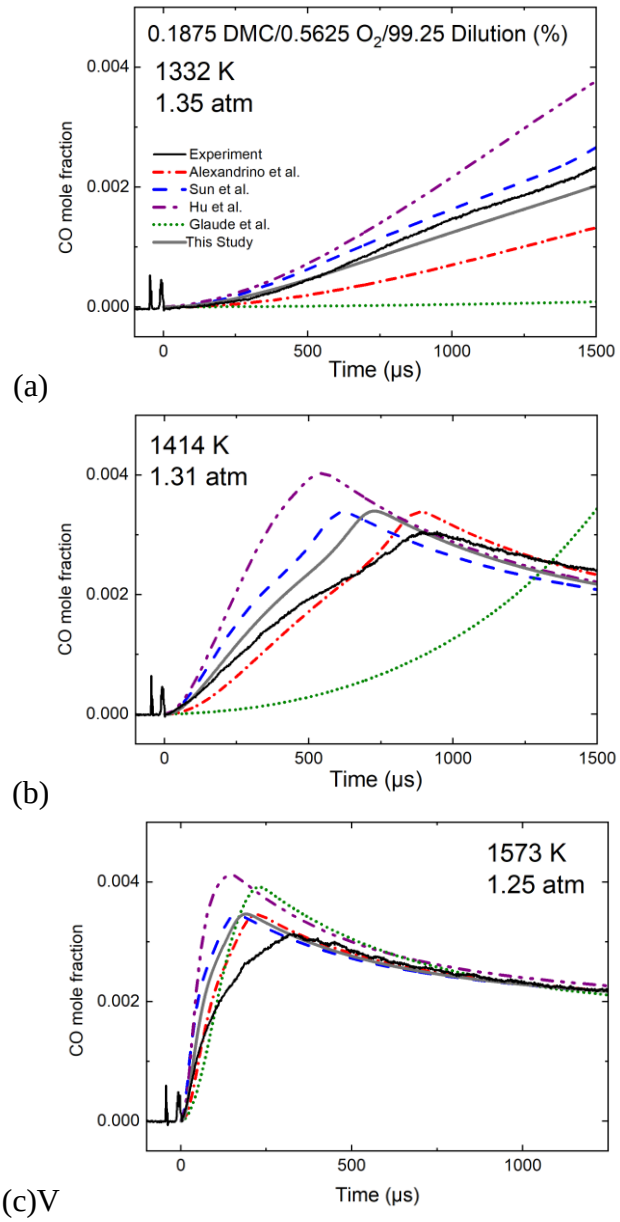

Figure 7. CO time histories and model comparison for φ = 1.0; (a) low-, (b) mid-, and (c) high- temperature cases.

When it comes to model comparison, the mechanisms considered can capture the overall shape of the measurements but differ in maximum CO formation and reactivity. The model from Hu et al. [8] is over-reactive and significantly over-predicts the amount of CO in all conditions. The Glaude et al. [7] model is also largely over-predicting CO,

but this model is significantly under-reactive. Note that the figures have been scaled to the experimental test-time for which the over-predictive behaviour of Glaude simulations cannot be fully seen for all cases, due to its under-reactivity; the low and mid temperature cases do produce a larger CO concentration but at a much later time. The two other models, Alexandrino et al. [10] and Sun et al. [9], offer better CO concentration predictions, although compared to the experimental values at the peak or plateau the two models are slightly higher by a factor of about 1.1, where the fuel-rich data was the closest to the model predictions. The Alexandrino model is slightly under-reactive by a factor around 0.8 for all cases but the stoichiometric condition where the model was over-reactive by a factor of 1.3. However, the Sun model tends to be over-reactive by an averaged factor of 1.3, for all cases, where the stoichiometric case shows the greatest deviation.

3.1.1.1. CO delay measurements

The delays to reach maximum carbon monoxide formation were measured in a similar manner to the one defined in Fig. 6 for OH* diagnostics. The effect that temperature has on the timing or delay reaching a peak can be better observed in Fig. 8. As shown, there is a logarithmic relationship between delay-to-peak and temperature, following an Arrhenius law relation, the shortest delay occur at the highest temperature and the opposite happens other way around for all cases. It can be observed that the Sun et al and Alexandrino et al. models can predict values closest to the experimental results and follow a similar logarithmic relation, as was the case for the model in This Study. On the other hand, the mechanisms of Glaude et al. and Hu et al. showed the most discrepancies

compared to the experimental data, behaviour observed across measured conditions. Furthermore, Fig. 8c shows how the model predictions at $\phi = 1.0$ are the farthest from the experimental data, compared to the fuel-lean and fuel-rich cases.

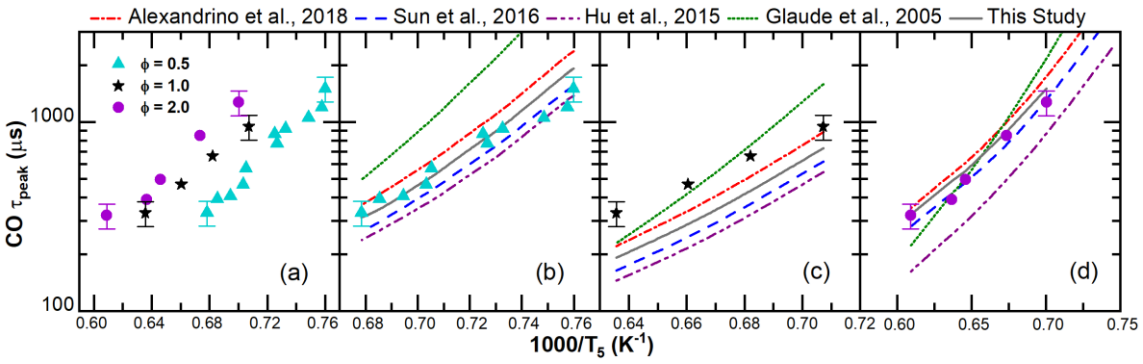

Figure 8. Time to peak maximum CO formation for DMC oxidation (lines: models, symbols: experimental results) (a) experimental results, (b), (c), and (d) model comparison at φ = 0.5, 1.0, and 2.0, respectively.

From a chemical kinetics standpoint, the shape of these CO profiles was expected. As shown in the curve, CO begins to form until it reaches a peak or maximum value, and as it decreases the system is undergoing CO_2 conversion, another common and expected combustion product. This maximum value was plotted versus T_5 for all experiments that reached a peak, as can be seen in Fig. 9. Note that only the Sun, Alexandrino, and tentative model of this study are close to the experimental data.

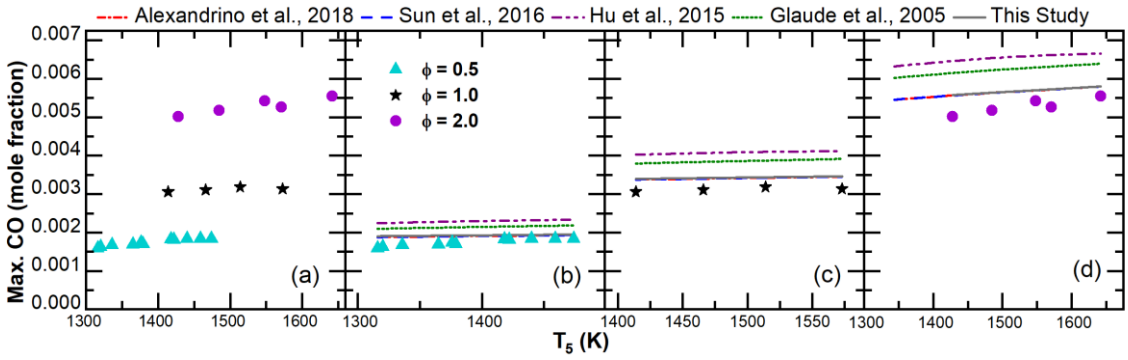

Figure 9. Maximum CO mole fraction versus T for DMC oxidation (lines: models, symbols: experimental results) (a) experimental results, (b), (c), and (d) model comparison at φ = 0.5, 1.0, and 2.0, respectively.

3.1.2. CO measurements for DMC pyrolysis

Contrary to the oxidation cases, after carbon monoxide formation phase, rather than reaching a peak, it converges to a plateau as shown in Figure 10. Nonetheless, the CO laser measurements from DMC pyrolysis also show how the rate at which CO forms decreases as the temperature increases.

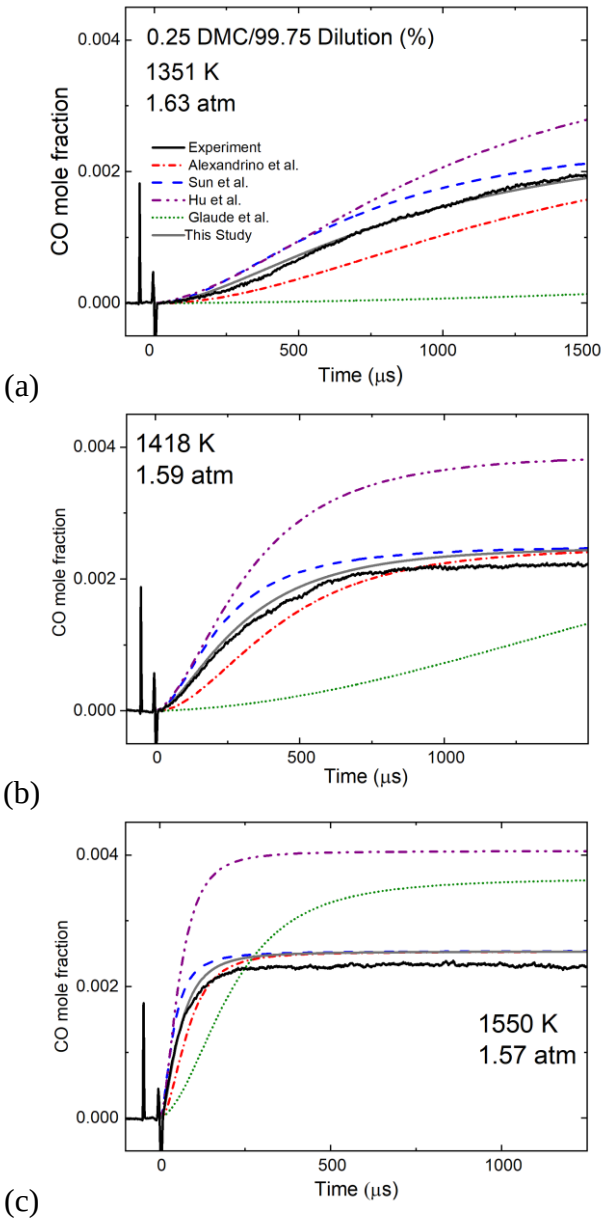

Figure 10. CO time histories and model comparison for φ = ∞; (a) low- , (b) mid-, and (c) high- temperature cases.

The experimental profiles allowed the assessments of effects of temperature and equivalence ratio across the data. It was observed that as temperature increases, the reactivity of CO formation increases. On the other hand, as the equivalence ratio increases, the amount of CO produced increases, Fig. 8, as expected. Another interesting observation

arose when comparing the effect of equivalence ratio at a similar temperature. The example shown in Fig. 11, compares the experimental data across all equivalence ratios investigated near 1420 K, showing this effect. As it can be seen the CO profile transitions from 1 peak to a 2-step process as ϕ increases for (a-c) in Figure 11, whereas no peak can be observed for the pyrolysis case.

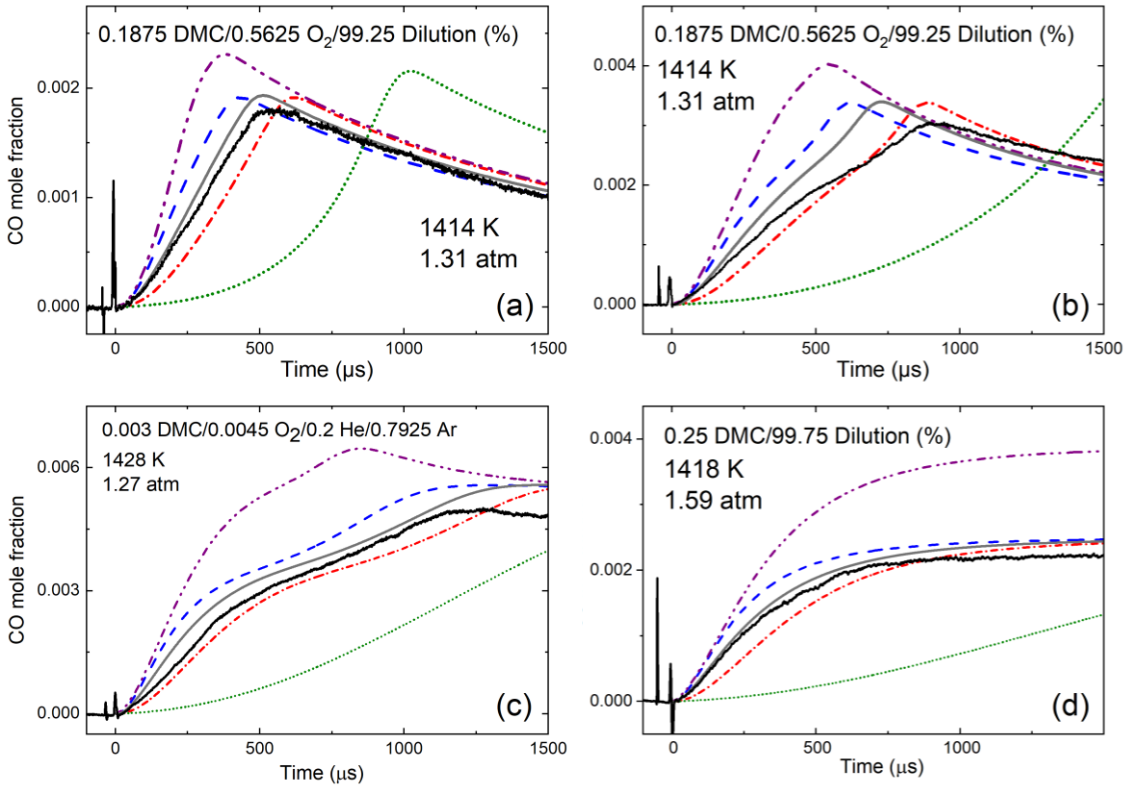

Figure 11. Effect of equivalence ratio at similar temperature from CO formation from DMC combustion for (a) φ = 0.5, (b) φ = 1.0, (c) φ = 2.0, and (d) φ = ∞.

3.2. Water (H_2O) Laser Absorption Measurements

Experimental and computed H_2O profiles for the oxidation and pyrolysis cases are presented in the subsequent subsections. Like the procedure used for CO, representative plots for the low, mid, and high temperatures are provided.

3.2.1. H_2O measurements for DMC oxidation

For the oxidation cases, the water formation starts at the very beginning of the experiment and eventually reaches a plateau. The time necessary to reach this plateau rapidly decreases with the increase in the temperature. All models are in good agreement with the experiments when it comes to predicting accurately the H_2O plateau values. Concerning the reactivity of the models in the presence of oxygen, the Hu and, to a lesser extent, Sun mechanisms are over-reactive except for the fuel-lean, high-temperature condition. The Glaude mechanism is consistently under-reactive, and the model from Alexandrino et al. [10] presents the best predictions overall, despite being under-reactive at low-to-intermediate temperatures.

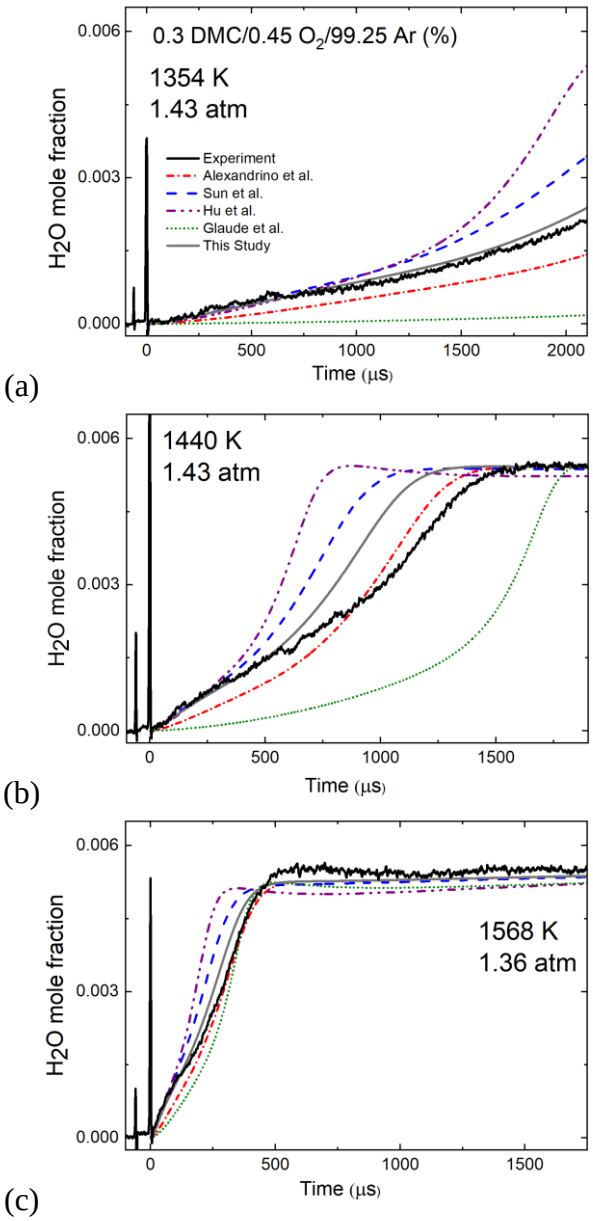

Figure 12. H_2O time histories and model comparison for φ = 2; (a) low- , (b) mid-, and (c) high- temperature cases.

3.2.2. H_2O measurements for DMC pyrolysis

The pyrolysis condition shows that only the Sun and Alexandrino models are able to predict accurately the experimental profiles, the two other models under-predict the

amount of water by approximately 70% in the time-frame of the experiments. Figure 13, illustrates the behaviour mentioned previously.

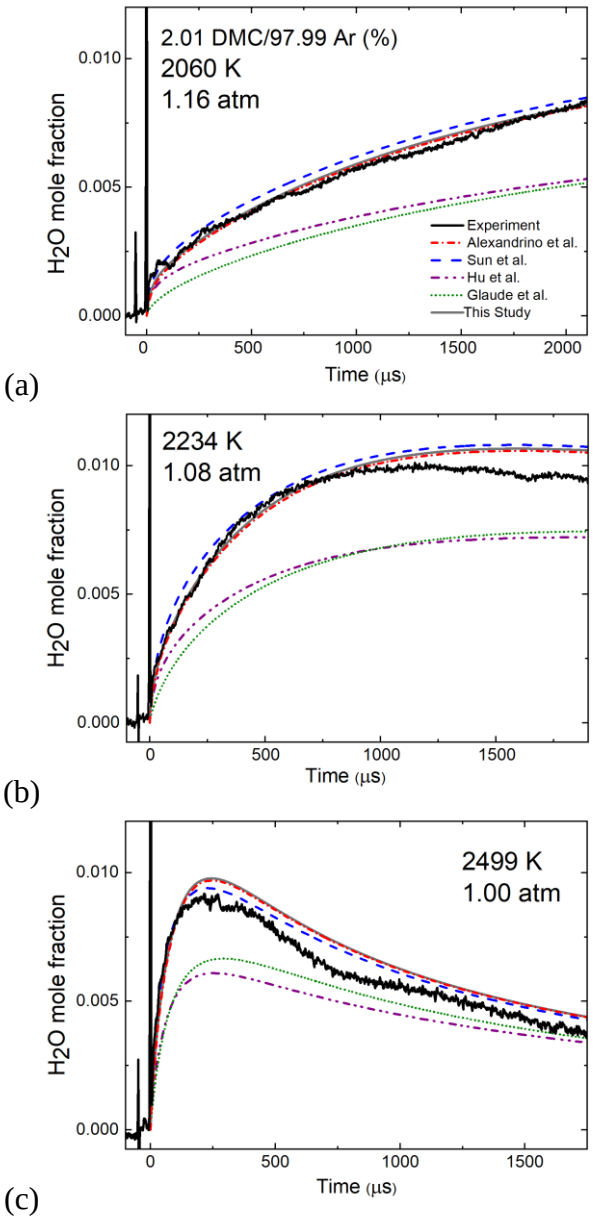

Figure 13. H_2O time histories and model comparison for φ = ∞; (a) low- , (b) mid-, and (c) high- temperature cases.

The effect of equivalence ratio has also been considered in a similar manner as was done for CO. Figure 14 depicts the fuel-lean and fuel-rich cases results, (a) and (b),

respectively, near 1440 K. As shown, the H_2O forms much faster as the fuel-lean case and produces approximately half of what is produced in the fuel-rich case.

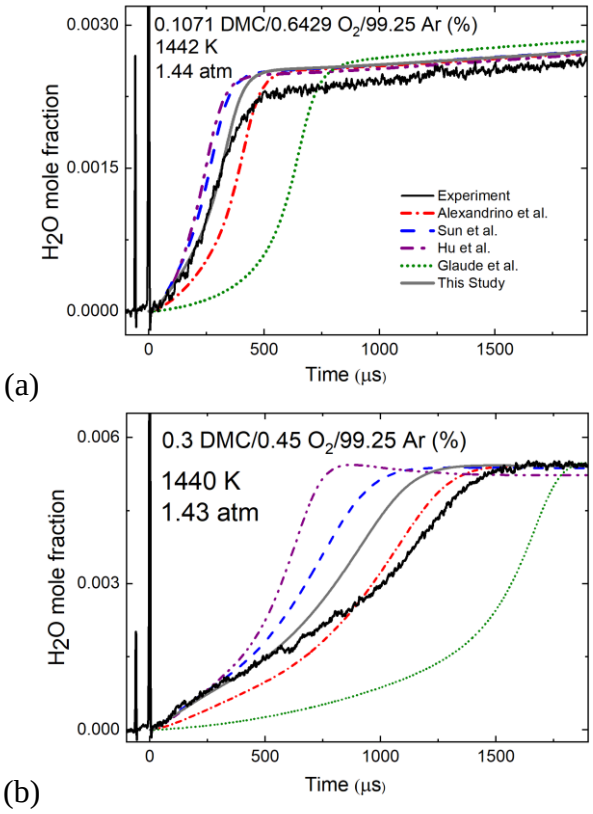

Figure 14. Comparison of (a) fuel-lean and (b) fuel-rich time histories near 1440 K.

3.3. Characteristic Time Delay Measurements

As can be seen in Fig. 15, τ_{peak} increases with ϕ and as the temperature decreases. A factor of about 1.5 is found for the time to peak OH* between the different equivalence ratios on the low-temperature side, and this factor is increasing with the temperature (a factor up to 2.2 between the fuel-lean and stoichiometric cases at 1475 K). The comparison with the models shows that the Glaude model is too slow, notably for the lower-

temperature conditions. Predictions from the Hu and Sun models are close, with the Sun model being closer to the data. These two models predict adequately τ_{peak} for the fuel-lean case but tend to be over-reactive for the other conditions, except for the coldest temperatures investigated. The Alexandrino model is slightly under-reactive at $\phi = 0.5$ by a factor of 0.7, but it is relatively accurate most of the time for the other conditions.

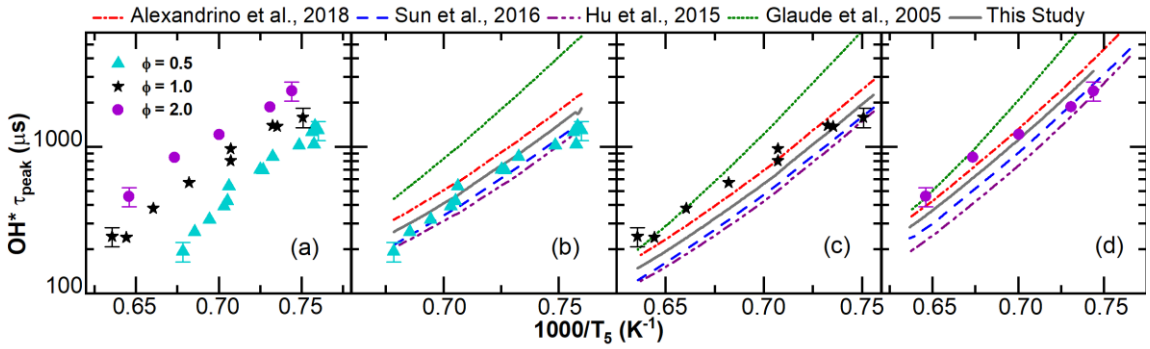

Figure 15. Characteristic reaction times for DMC oxidation (lines: models, symbols: experimental results) (a) experimental results, (b), (c), and (d) model comparison at $\phi = 0.5$, 1.0, and 2.0, respectively.

3.4. Laminar Flame Speed Measurements

3.4.1. Laminar Flame Speed Vessel

Laminar flame speeds ($S_{L,u}^0$) were measured in a double-walled spherical vessel, with an internal diameter of 476 mm. Between the two spheres, a heat transfer fluid heats the apparatus to the desired temperature (318, 363, and 423K, with a ±1 K homogeneity). The pressure during combustion was monitored using a piezo-electric transducer (Kistler 601A). Mixtures were spark-ignited with two tungsten electrodes and a high-voltage generator, with an average energy delivery of 1.82 mJ with a standard deviation of 0.48

mJ. Mixtures (initial pressure of 1.013 bar) were prepared inside the vessel using the partial pressure method with anhydrous DMC (Sigma Aldrich® ≥99%) and dry air (Air Liquide, alphagaz 1®, 21% O_2/79% N_2, 99.999% purity). A photograph of the experimental setup and schematic of diagnostic setup can be found in Figures 16 and 17, respectively. As previously mentioned, the information gathered in this subsection is courtesy of Dr. Chaumeix.

Figure 16. Laminar Flame Speed Facility at ICARE, CNRS, Orléans, France. Obtained directly from [31, 32].

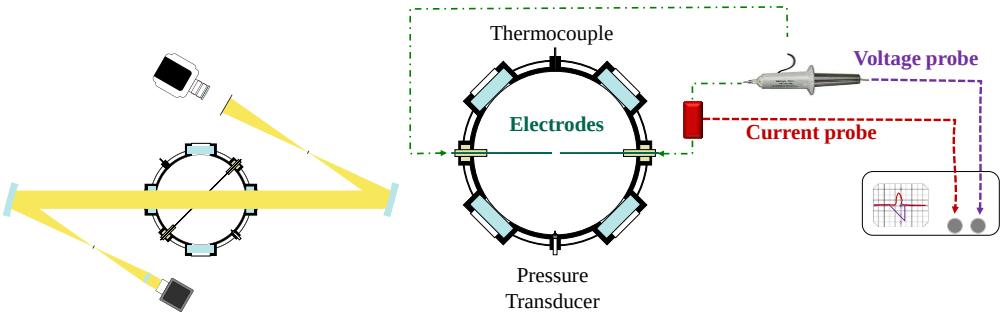

Figure 17. CNRS measuring instruments setup. Taken directly from [31, 32].

Pressures were measured using capacitance manometers (MKS, 0-100 and 0-1000 Torr). The spherical bomb is equipped with two opposing quartz windows (100-mm diameter, 50-mm thick), allowing for flame visualization using a Z-type schlieren apparatus. A white continuous lamp was used to illuminate the flame via two lenses and concave spherical mirrors. The schlieren images of the growing flame were recorded using a high-speed camera (PHANTOM V1610, 25000 fps, 768×768 pixels^2, fixed frame size).

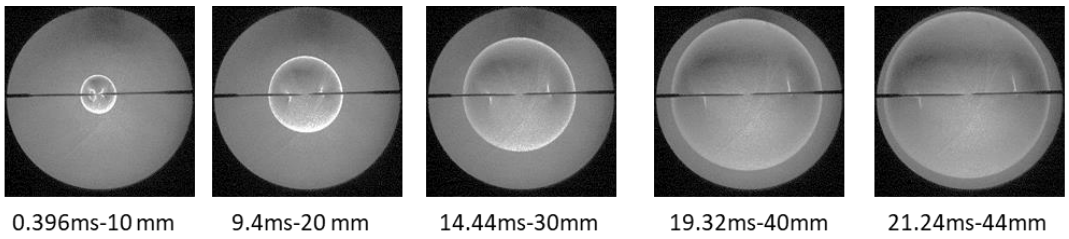

Figure 18. Typical Laminar Flame Speed propagation. Sample experiment at ϕ = 0.9, T0 = 318 K and 1 bar. Obtained directly from [31, 32].

Images were processed using a home-made MATLAB code to obtain the flame radius (R_f) as a function of time, from which the spatial (burned gas) flame speed $V_S=dR_f/dt$ could be determined. Figure 18 provides an example of the times and distances obtained during the flame propagation imaging of an experiments at 318 K near 1 atm. A stretch correction to the velocity either using a non-linear or a linear extrapolation was used. For this study, all the unstretched spatial flame speeds between 10 mm and about 42 mm were extrapolated using the non–linear extrapolation from Ronney and Sivashinsky [30]. Since the spherical bomb allows the recording of large flames without any effect of the vessel,

the laminar flame speed at zero-stretch is not affected by the extrapolation method, as shown in Figure 19.

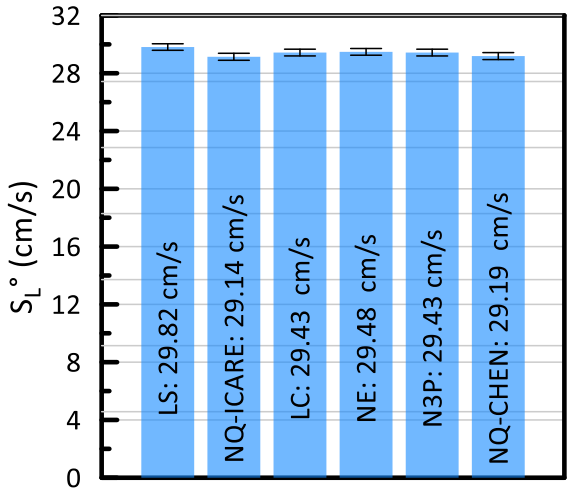

Figure 19. Laminar flame speed at zero-stretch according to the extrapolation method for ϕ = 0.93 at an initial temperature of 318 K. The extrapolation methods are: LS, linear; NQ, quasi-steady non-linear, LC, linear based on curvature; N3P, non-linear [31, 32].

The lowest radius was chosen to avoid any history from the ignition and the largest to avoid any pressure or wall effects. The observed burned volume is about 0.8% of the vessel volume, and the pressure remains constant during the visualization of the flame. More details can be found in [31, 32], schematics of the apparatus and representative flame images are available in Supplemental Material.

3.4.2. Flame speed model assessment

Laminar flame speed experiments were conducted at an initial pressure of 1.0 atm, for equivalence ratios ranging from 0.7 to 1.5. The limits were chosen to ensure successful ignition and to avoid flame wrinkling, respectively. Figure 20a shows the evolution of

unstretched laminar flame velocity ($S_{L,u}^0$) of DMC/air mixtures for several initial temperatures as a function of ϕ. It is visible that $S_{L,u}^0$ notably increases with the initial temperature, with maximum values reached at ϕ=1.1 (31.4, 38.7, and 51.4 cm/s at 318, 363, and 423 K, respectively).

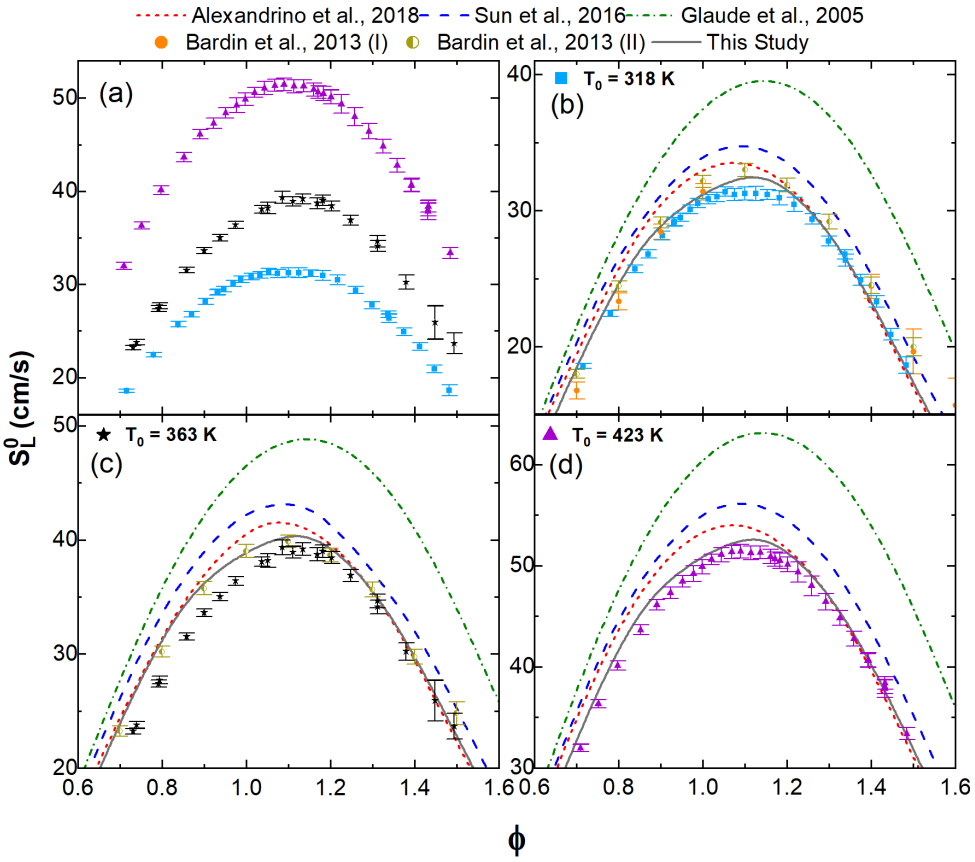

Figure 20. $S_{L,u}^0$ for DMC/air mixtures at P = 1.013 bar. (Symbols: Experimental data, lines: Models) (a) experimental results, (b), (c), and (d) model comparison at 318, 363, and 423 K, respectively.

Results at 318 K (Fig. 20b) and 363 K (Fig. 20c) were compared with data from Bardin et al. [33], measured at 318 and 358 K on two experimental setups (denoted I and II). The present data are in reasonable agreement with the literature data, with the best agreement

obtained with measurements from their first setup. Some discrepancies can be observed with the results from their second setup, with the present $S_{L,u}^{0}$ being consistently slower by about 2 cm/s. This discrepancy could be explained by various reasons such as the difference in the methods (heat flux burner vs spherical bomb [33]), the initial temperature uncertainty and/or the O_2/N_2 ratio between the two types of experiments.

Laminar flame speed modelling was performed using the Glaude, Sun, and Alexandrino models only, since no transport data were provided by Hu et al. [8]. As seen in Fig. 6, the models are capturing the experimental trends with the change in temperature and equivalence ratio, but they predict flame speeds that are too high in most cases. This observation is indeed the case for the Glaude model, for all conditions. The Sun model also over-predicts the maximum flame speed by a factor of 1.11, but is only slightly above the experimental error for 318 K and 423 K by a factor of 1.15 and 1.09 on the fuel-lean and fuel-rich sides, respectively. For 363 K, Sun model is over-predictive by a factor up to 1.24 on the fuel-lean side, while it shows the least deviation from the experimental data on the fuel-rich side with a factor of 0.87. Finally, the tentative model shown as "This Study" in the figures (discussed below) is the closest to the data, with the most accurate predictions occurring on the fuel-rich side. As depicted in Figure 20, the tentative model is not only closer to the experimental data than the other models in terms of maximum flame speed, but this maximum is now slightly shifted towards the fuel rich side too, closer to the experiments.

3.5. Sensitivity Analysis

All simulation-related computational analysis presented in this study was performed using ANSYS Chemkin Pro package from Reaction Design [34]. These computations include a priori experimental predictions, model simulations and sensitivity analysis assuming a closed homogeneous reactor mode, constrained volume and solving for energy equations. Chemkin Pro enabled the determination of important reactions in the DMC sub mechanism needing some revisiting/recalculations. This was possible as the program estimates the reactions driving the formation of a target species, in this case, CO and H_2O under given experimental conditions. The sensitivity analysis consists of finding the sensitivity coefficient of every single reaction in the detailed chemical kinetics model used for the computational simulations. Noting, that the calculations during simulations were computed at every time step, set to 1 microsecond, to match the experimental data acquisition sampling rate. A representation of this analysis with normalized sensitivity coefficients for mid-temperature case can be found in Fig. 21.

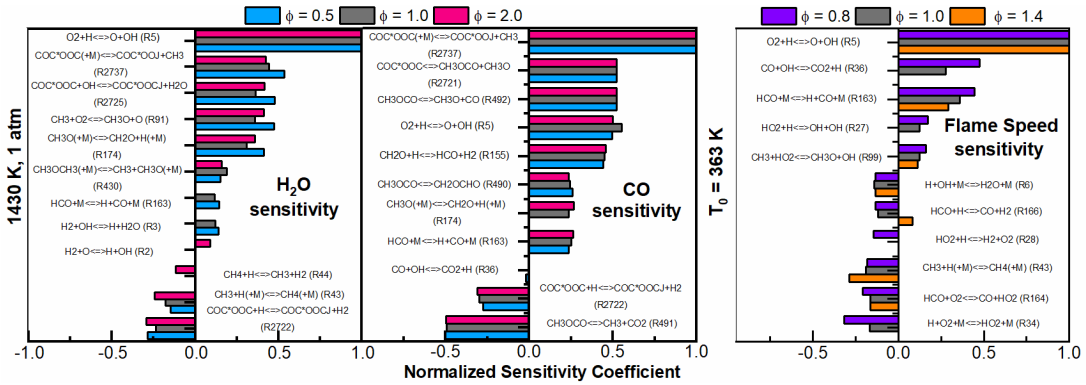

Figure 21. Normalized sensitivity coefficients at intermediate temperature for shock-tube species concentration and laminar flame speed measurements using the model from Alexandrino et al. [10].

Overall, the results presented herein showed that the model from Alexandrino et al. [10] was the most accurate. Using this model, a sensitivity analysis was conducted for $S_{L,u}^{0}$, and also for the CO and H_2O profiles, for the three studied equivalence ratios and for an intermediate temperature at atmospheric pressure (Fig. 21). A sensitivity analysis was performed for the tentative model, showing no significant differences from the overall trends depicted by the Alexandrino et al. mechanism.

3.6. Chemical Kinetics Mechanism

As mentioned previously, the tentative model presented in this study was originated from the Alexandrino et al. mechanism, as it was determined to be the most accurate literature model overall. This model was first updated by and substituting the AramcoMech2.0 by AramcoMech3.0 [35] for the chemistry that was not related to DMC. The author used the CO, H_2O and OH* experimental profiles jointly with the laminar flame data to adjust the reaction rate of three key reactions of the DMC sub-mechanism, these reactions being determined using sensitivity analysis as described below.

For the shock-tube results, Fig. 21, besides the well-characterized reactions pertaining to the so-called base chemistry (constituting all of the flame speed analysis), this analysis exhibited three important reactions involving DMC (COC*OOC in the model):

$$COC^*OOC(+M) \leftrightarrows COC^*OOj + CH_3(+M) \quad (R2737)$$

$$COC^*OOC + H \leftrightarrows COC^*OOCj + H_2 \quad (R2722)$$

$$COC^*OOC + OH \leftrightarrows COC^*OOCj + H_2O \quad (R2725)$$

referring to the reaction numbers in the Alexandrino et al. model. The reactions R2722, R2725, and R2737, were then modified by adjusting their pre-exponential factor, with the present data as targets. To summarize, the optimum solution was found with the following adjustments of the pre-exponential factors: k_{R2737}×1.54, k_{R2722}/2, and k_{R2725}×3. Results from this tentative model are presented in Figs. 7-15, 20 and have been discussed already. To summarize, the resulting predictions are notably improved for both the shock-tube and $S_{L,u}^0$ results. These adjustments can be justified by the fact that the reaction rate of these specific reactions in the DMC sub-mechanism are not very well characterized, as detailed below.

It must be noted that other shock tube related studies from literature such were also considered in this study, including reacting rates determined in work of authors such as Peukert et al. [36] and Khaled et al. [37]. R2737 (COC*OOC(+M) ⇆ COC*OOj + CH_3(+M)) is of primary importance for shock-tube results, and Alexandrino et al. utilized the reaction rate proposed by Dooley et al. [38], estimated for a similar reaction with methyl-butanoate [38] (based on ignition delay time measurements), on the account that the reaction rate is in "reasonable agreement" with the one determined by Peukert et al. [36] for DMC and that methyl-butanoate presents a similar chemical structure. For reaction R2722 (COC*OOC + H ⇆ COC*OOCj + H_2), Alexandrino et al. used the rate employed in Sun et al. [9], which is the reaction rate proposed by Peukert and coworkers [36]. Finally, for R2725 (COC*OOC + OH ⇆ COC*OOCj + H_2O), Alexandrino et al. used the rate proposed by Sun et al., which has been assessed by analogy with a similar reaction with methyl-formate [39]. Note that R2725 has been recently studied by Khaled

et al. [26], both experimentally and by high-level calculation. Two corresponding reaction rates were determined near 1.5 atm. The reaction rate deriving from the experimental data was determined between 872 and 1295 K whereas the calculated reaction rate was determined in the 300-1500 K range. A graph of the evolution of the various reaction rates for R2725 versus the temperature is visible in Appendix section.

Note that for the highest temperature investigated herein, 2500 K, the reaction rate proposed in this study is close (and within the uncertainty) to the calculated rate from Khaled et al., only 14% higher, and it is worth mentioning that the experimental rate is also slightly higher than the value used in the Alexandrino model. On the low temperature side of our conditions, the experimental rate of Khaled et al. and the one from the Alexandrino model are close, within 13%, making the rate for the tentative model 3 times higher overall (considered as the higher limit of the uncertainty). Note also that the calculated rate significantly diverges at this low temperature. It is worth mentioning that the rates from Khaled et al. were both alternatively used in the tentative model and the Alexandrino model, and none were improving the predictions (figures included in Appendix).

In the author's opinion, this discussion is a good indicator of the future work that is necessary to better determine directly, either experimentally and/or by high-level calculations, the rate of the few reactions that involve DMC, and, as such, the tentative model cannot be used to confidently model DMC combustion chemistry too far from the conditions investigated herein.

4. CONCLUSIONS AND RECOMMENDATION*

New global ($\tau_{peak}, S_{L,u}^{0}$) and fundamental (H_2O and CO time histories) experiments were performed to investigate Dimethyl-carbonate, or DMC, combustion chemistry near atmospheric pressure. DMC is currently being employed in a wide spectrum of applications, such as biofuel additive for Diesel engines and as part of the mixture of solvents that make the electrolyte component in LIBs. DMC is a highly oxygenated fuel that has gained interest in industry and research due to its promising characteristics such as soot reduction without having an effect in NOx in diesel engines and to its "green" way of producing it, *i.e.*, direct synthesis from methanol and CO_2. However, the high flammability of species like DMC can pose a real-life problem in applications such as EVs reporting fire incidents in their battery cell pack.

Few kinetics data are available in the literature for DMC, and the species time histories and laminar flame speed data obtained in the present study are the first of their kind for DMC, to the author's knowledge. These data were compared to several detailed kinetics models from the literature. None of the models however were able to adequately predict the data over the entire range of conditions investigated, and the new data obtained herein can be used to improve the chemistry of DMC combustion.

---

* Parts of this section are reprinted with permission from "Laminar flame speed and shock-tube multi-species laser absorption measurements of Dimethyl Carbonate oxidation and pyrolysis near 1 atm" by Atherley, T., de Persis, S., Chaumeix, N., Fernandes, Y., Bry, A., Comandini, A., Mathieu, O., Alturaifi, S., Mulvihill, C. R., Petersen, E. L., 2021, *Proceedings of the Combustion Institute*, Vol. 38, pp. 977-985, Copyright 2020 The Combustion Institute. Published by Elservier Inc. https://doi.org/10.1016/j.proci.2020.06.333

Sensitivity and reaction pathway analyses were performed with the most-accurate model, allowing the identification of key reactions involving DMC. The rate of these reactions was reasonably modified, and a tentative model was proposed. Despite the fact the flame speed results were in general sensitive to well-characterized reactions from the base chemistry, the changes in the DMC reactions did have an impact on the flame speed results but to a lesser extent than the shock-tube data. It was found possible to greatly improve the predictions by using this tentative model, indicating a great need to further study the rate of the three reactions modified.

The present real-life occurrences remind the reader that combustion concerns should not be overlooked. Fundamental chemical kinetics mechanisms developed can aid in the process of understanding the problem and identifying solutions, with tools such as fire suppressants or improved models for predictions. This study explored the chemical kinetics of DMC combustion, by first assessing the models available in the literature, comparing experimental results with the literature, and found that there is a need for further model validation.

It is worth mentioning that this work was used to demonstrate the feasibility of this type of studies in a proposal that has since been accepted by the National Science Foundation. This future work in the laboratory of Dr. Petersen will focus on other components of LIBs' electrolyte as well as some potential fire suppressant. Beyond that, the future work should be guided towards more thorough reaction rate chemical kinetics analysis and determination of reaction rate coefficients based on the presented experimental work, in aims of improving the tentative model presented herein. Increasing

the means of safety for LIBs have been known to be a coming challenge, specially at the rate at which these technologies are developed. Li-air and Li-sulfur systems are examples of potential competitors to current LIB technology. As the world envisions a transition to more efficient means of energy usage, mass adoption of new technology is to be expected, although this should be done after all parameters have been considered/tested/analyzed to ensure public safety.

REFERENCES

[1] Tamboli, A.H., Chaugule, A.A., Kim, H., "Catalytic developments in the direct dimethyl carbonate synthesis from carbon dioxide and methanol", *Chemical Engineering Journal*, Vol. 323, 2017, pp. 530-544.

[2] Alzueta, M.U., Salinas, P., Millera, Á., Bilbao, R., Abián, M., "A study of dimethyl carbonate conversion and its impact to minimize soot and NO emissions", *Proceedings of the Combustion Institute*, Vol. 36, 2017, pp. 3985-3993.

[3] Abdalla, A.O.G., Liu, D., "Dimethyl carbonate as a promising oxygenated fuel for combustion: A review", *Energies*, Vol. 11, 2018, pp. 1552.

[4] Wang, Q., Mao, B., Stoliarov, S.I., Sun, J., "A review of lithium ion battery failure mechanisms and fire prevention strategies", *Progress in Energy and Combustion Science*, Vol. 73, 2019, pp. 95-131.

[5] Harris, S.J., Timmons, A., Pitz, W.J., "A combustion chemistry analysis of carbonate solvents used in Li-ion batteries", *Journal of Power Sources*, Vol. 193, 2009, pp. 855-858.

[6] Fernandes, Y., Bry, A., de Persis, S., "Identification and quantification of gases emitted during abuse tests by overcharge of a commercial Li-ion battery", *Journal of Power Sources*, Vol. 389, 2018, pp. 106-119.

[7] Glaude, P.A., Pitz, W.J., Thomson, M.J., "Chemical kinetic modeling of dimethyl carbonate in an opposed-flow diffusion flame", *Proceedings of the Combustion Institute*, Vol. 30, 2005, pp. 1111-1118.

[8] Hu, E., Chen, Y., Zhang, Z., Pan, L., Li, Q., Cheng, Y., Huang, Z., "Experimental and kinetic study on ignition delay times of dimethyl carbonate at high temperature", *Fuel*, Vol. 140, 2015, pp. 626-632.

[9] Sun, W., Yang, B., Hansen, N., Westbrook, C.K., Zhang, F., Wang, G., Moshammer, K., Law, C.K., "An experimental and kinetic modeling study on dimethyl carbonate (DMC) pyrolysis and combustion", *Combustion and Flame*, Vol. 164, 2016, pp. 224-238.

[10] Alexandrino, K., Alzueta, M.U., Curran, H.J., "An experimental and modeling study of the ignition of dimethyl carbonate in shock tubes and rapid compression machine", *Combustion and Flame*, Vol. 188, 2018, pp. 212-226.

[11] Guo, F., Hase, W., Ozaki, Y., Konno, Y., Inatsuki, M., Nishimura, K., Hashimoto, N., Fujita O., "Experimental study on flammability limits of electrolyte solvents in lithium-ion batteries using a wick combustion method", *Experimental Thermal and Fluid Science*, Vol. 109, 2019, pp. 109858.

[12] Diaz, F., Wang, Y., Weyhe, R, Friedrich, B., "Gas generation measurement and evaluation during mechanical processing and thermal treatment of spent Li-ion batteries", *Waste Management*, Vol. 84, 2019, pp. 102–111.

[13] Stephens, D., Shawcross, P., Stout, G., Sullivan, E., Saunders, J., Risser, S., Sayre, J., "Lithium-ion battery safety issues for electric and plug-in hybrid vehicles" Report No. DOT HS 812 418, 2017, Washington, DC: National Highway Traffic Safety Administration.

[14] Wang, Q., Mao, B., Stoliarov, S. I., Sun, J., “A review of lithium ion battery failure mechanisms and fire prevention strategies”, *Progress in Energy and Combustion Science*, Vol. 73, 2019, pp. 95–131.

[15] Henze, V., “Battery Pack Prices Cited Below $100/kWh for the First Time in 2020, While Market Average Sits at $137/kWh.”, BloombergNEF, December 16, 2020. https://about.bnef.com/blog/battery-pack-prices-cited-below-100-kwh-for-the-first-time-in-2020-while-market-average-sits-at-137-kwh/

[16] Kaneva, N., “Driving into 2025: The Future of Electric Vehicles.”, J.P. Morgan, October 10, 2018. Retrieved online: April 2019, https://www.jpmorgan.com/global/research/electric-vehicles

[17] “Global EV Outlook 2020”, IEA Technology Report, June, 2020. https://www.iea.org/reports/global-ev-outlook-2020

[18] Ghosh P., “Hyundai to recall 76000 Electric Vehicles Over Battery Fire Risk”. Forbes, February 24, 2021. https://www.forbes.com/sites/palashghosh/2021/02/24/hyundai-to-recall-76000-electric-vehicles-over-battery-fire-risks/?sh=42f726622cf5

[19] Madway G., Hamada. K., Negishi, M., Takenaka, K., Joyce, R., “Sony recalls PC batteries”, Reuters, October 31, 2008. Press release available at: https://www.reuters.com/article/us-sony%20battery/sony-recalls-pc-batteries-idUSTRE49U1EZ20081031

[20] “Samsung Expands Recall of Galaxy Note7 Smartphones Based on Additional Incidents with Replacement Phones; Serious Fire and Burn Hazards.” United

States Consumers Product Safety Commission, October, 2016, available at: https://www.cpsc.gov/Recalls/2016/samsung-expands-recall-of-galaxy-note7-smartphones-based-on-additional-incidents-with

[21] Petersen, E.L., Rickard, M.J.A., Crofton, M.W., Abbey, E.D., Traum, M.J., Kalitan, D.M., "A facility for gas- and condensed-phase measurements behind shock waves", *Measurement Science and Technology*, Vol. 16, 2005, pp. 1716-1729.

[22] Mathieu, O., Mulvihill, C.R., Petersen, E.L., "Assessment of modern detailed kinetics mechanisms to predict CO formation from methane combustion using shock-tube laser-absorption measurements", *Fuel*, Vol. 236, 2019, pp. 1164-1180.

[23] Rothman, L.S., Jacquemart, D., Barbe, A., Chris Benner, D., Birk, M., Brown, L.R., Carleer, M.R., Chackerian, C., Chance, K., Coudert, L.H., Dana, V., Devi, V.M., Flaud, J.M., Gamache, R.R., Goldman, A., Hartmann, J.M., Jucks, K.W., Maki, A.G., Mandin, J.Y., Massie, S.T., Orphal, J., Perrin, A., Rinsland, C.P., Smith, M.A.H., Tennyson, J., Tolchenov, R.N., Toth, R.A., Vander Auwera, J. , Varanasi, P., Wagner, G., "The HITRAN 2004 molecular spectroscopic database", *Journal of Quantitative Spectroscopy and Radiative Transfer*, Vol. 96, 2005, pp. 139-204.

[24] Ren, W., Farooq, A., Davidson, D.F., Hanson, R.K., "CO concentration and temperature sensor for combustion gases using quantum-cascade laser absorption near 4.7 μm", *Applied Physics B*, Vol. 107, 2012, pp. 849-860.

[25] Nagali, V., Davidson, D.F., Hanson, R.K., "Measurements of temperature-dependent argon-broadened half-widths of H2O transitions in the 7117 cm−1 region", *Journal of Quantitative Spectroscopy and Radiative Transfer*, Vol. 64, 2000, pp. 651-655.

[26] Mulvihill, C.R., Keesee, C.L., Sikes, T., Teixeira, R.S., Mathieu, O., Petersen, E.L., "Ignition delay times, laminar flame speeds, and species time-histories in the H2S/CH4 system at atmospheric pressure", *Proceedings of the Combustion Institute*, Vol. 37, 2019, pp. 735-742.

[27] Mathieu, O., Mulvihill, C., Petersen, E.L., "Shock-tube water time-histories and ignition delay time measurements for H2S near atmospheric pressure", *Proceedings of the Combustion Institute*, Vol. 36, 2017, pp. 4019-4027.

[28] Urzay, J., Kseib, N., Davidson, D.F., Iaccarino, G., Hanson, R.K., "Uncertainty-quantification analysis of the effects of residual impurities on hydrogen–oxygen ignition in shock tubes", *Combustion and Flame,* Vol. 161, 2014, pp. 1-15.

[29] Mulvihill, C. R., Petersen E. L., "Concerning shock-tube ignition delay times: An experimental investigation of impurities in the H_2/O_2 system and beyond", *Proceedings of the Combustion Institute*, Vol. 37, 2019, pp. 259-266.

[30] Ronney, P.D., "On the mechanisms of flame propagation limits and extinguishment-processes at microgravity", *Proceedings of the Combustion Institute,* Vol. 22, 1989, pp. 1615-1623.

[31] Grosseuvres, R., Comandini, A., Bentaib, A., Chaumeix, N., "Combustion properties of H2/N2/O2/steam mixtures", *Proceedings of the Combustion Institute*, Vol. 37, 2019, pp. 1537-1546.

[32] Nativel, D., Pelucchi, M., Frassoldati, A., Comandini, A., Cuoci, A., Ranzi, E., Chaumeix, N., Faravelli, T., "Laminar flame speeds of pentanol isomers: An experimental and modeling study", *Combustion and Flame*, Vol. 166, 2016, pp. 1-18.

[33] Bardin, M.E., Ivanov, E.V., Nilsson, E.J.K., Vinokurov, V.A., Konnov, A.A., "Laminar burning velocities of dimethyl carbonate with air", *Energy & Fuels*, Vol. 27, 2013, pp. 5513-5517.

[34] CHEMKIN-PRO 18.0, Ansys, 2018.

[35] Zhou, C.-W., Li, Y., Burke, U., Banyon, C., Somers, K.P., Ding, S., Khan, S., Hargis, J.W., Sikes, T., Mathieu, O., Petersen, E.L., AlAbbad, M., Farooq, A., Pan, Y., Zhang, Y., Huang, Z., Lopez, J., Loparo, Z., Vasu, S.S., Curran, H.J., "An experimental and chemical kinetic modeling study of 1,3-butadiene combustion: Ignition delay time and laminar flame speed measurements", *Combustion and Flame*, Vol. 197, 2018, pp. 423-438.

[36] Peukert, S.L., Sivaramakrishnan, R., Michael, J.V., "High Temperature Shock Tube and Theoretical Studies on the Thermal Decomposition of Dimethyl Carbonate and Its Bimolecular Reactions with H and D-Atoms", *Journal of Physical Chemistry A*, Vol.117, 2013, pp. 3718-3728.

[37] Khaled, F., Giri, B.R., Szőri, M., Mai, T.V.T., Huynh, L.K., Farooq, A. “A combined high-temperature experimental and theoretical kinetic study of the reaction of dimethyl carbonate with OH radicals”, *Physical Chemistry Chemical Physics*, Vol. 19, 2017, pp. 7147-7157.

[38] Dooley, S., Curran, H.J., Simmie, J.M., “Autoignition measurements and a validated kinetic model for the biodiesel surrogate, methyl butanoate”, *Combustion and Flame*, Vol. 153, 2008, pp. 2-32.

[39] Dooley, S., Burke, M.P., Chaos, M., Stein, Y., Dryer, F.L., Zhukov, V.P., Finch, O., Simmie, J.M., Curran, H.J., “Methyl formate oxidation: Speciation data, laminar burning velocities, ignition delay times, and a validated chemical kinetic model”, *International Journal of Chemical Kinetics*, Vol. 42, 2010, pp. 527-549.

APPENDIX A

SUPPLEMENTAL MATERIAL

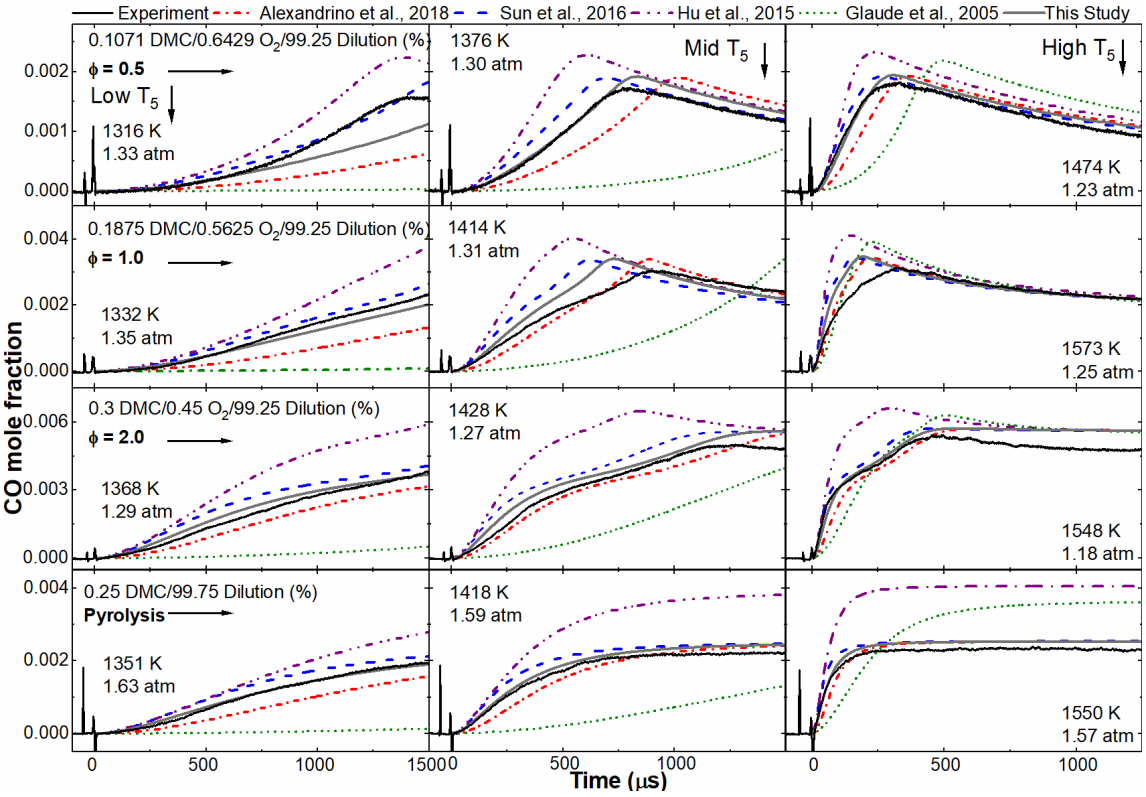

Figure A.1. CO time histories and model comparisons for DMC oxidation and pyrolysis.

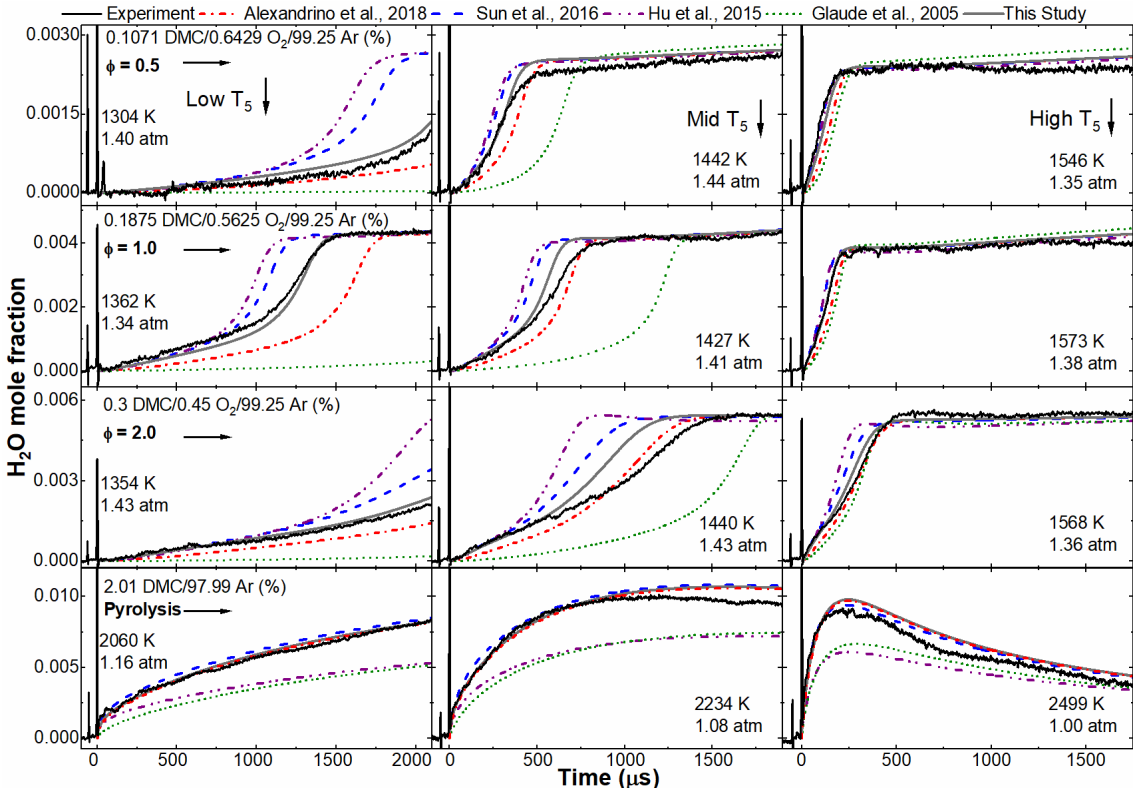

Figure A.2. H2O time histories and model comparisons for DMC oxidation and pyrolysis.

1. CO time histories

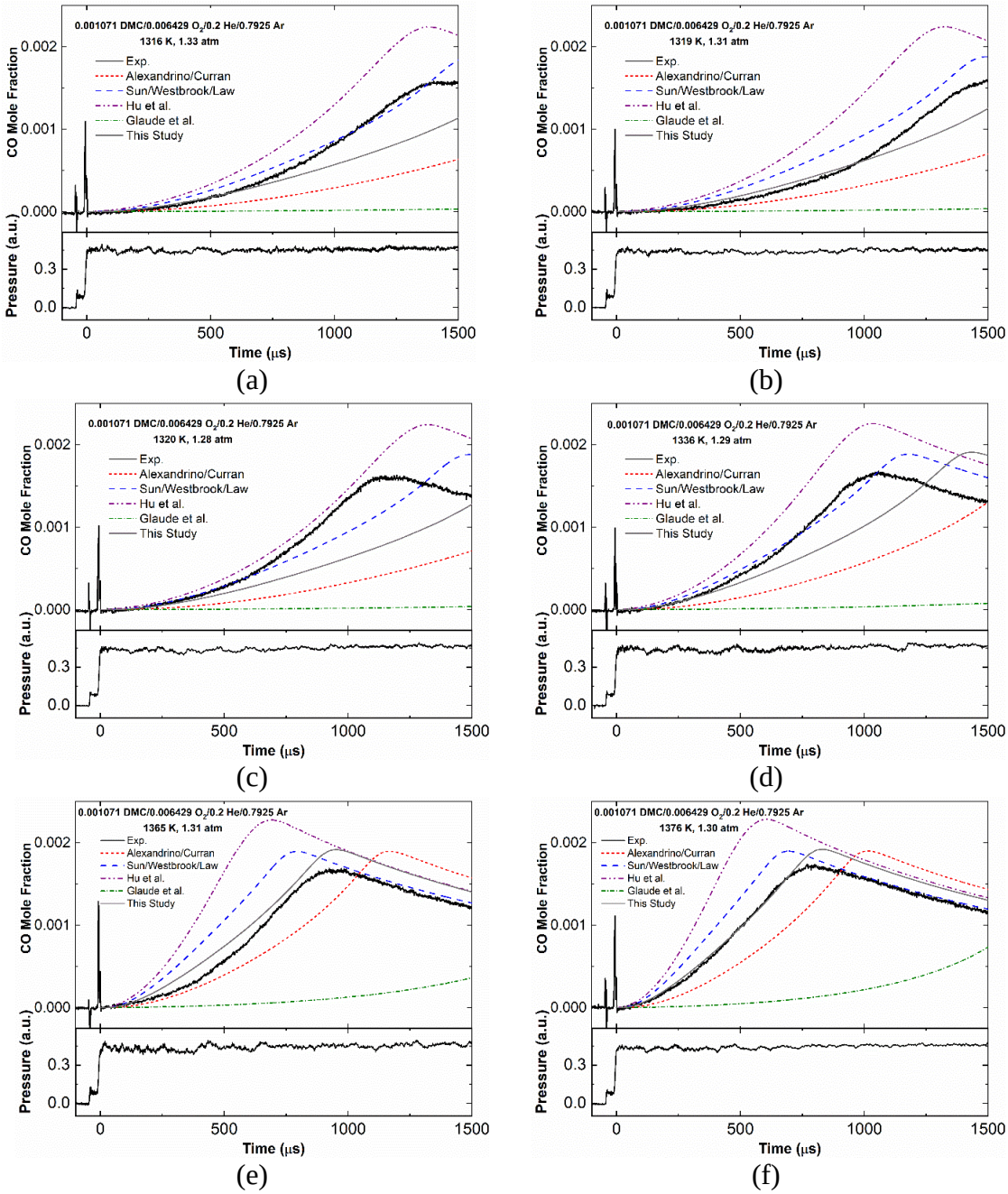

Figure A.3. CO time histories and model comparison for $\phi = 0.5$.

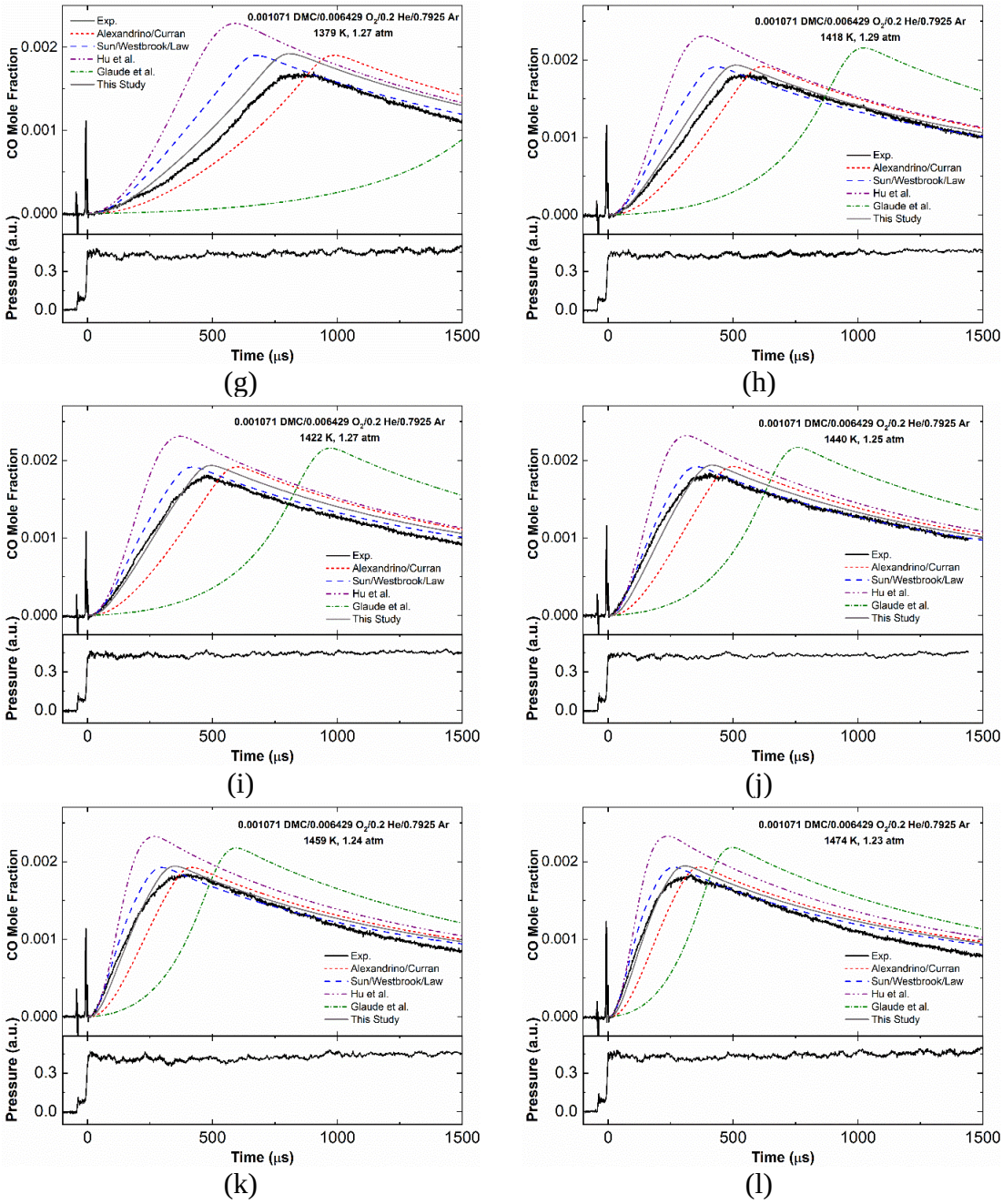

Figure A.3. CO time histories and model comparison for ϕ = 0.5 – Continued.

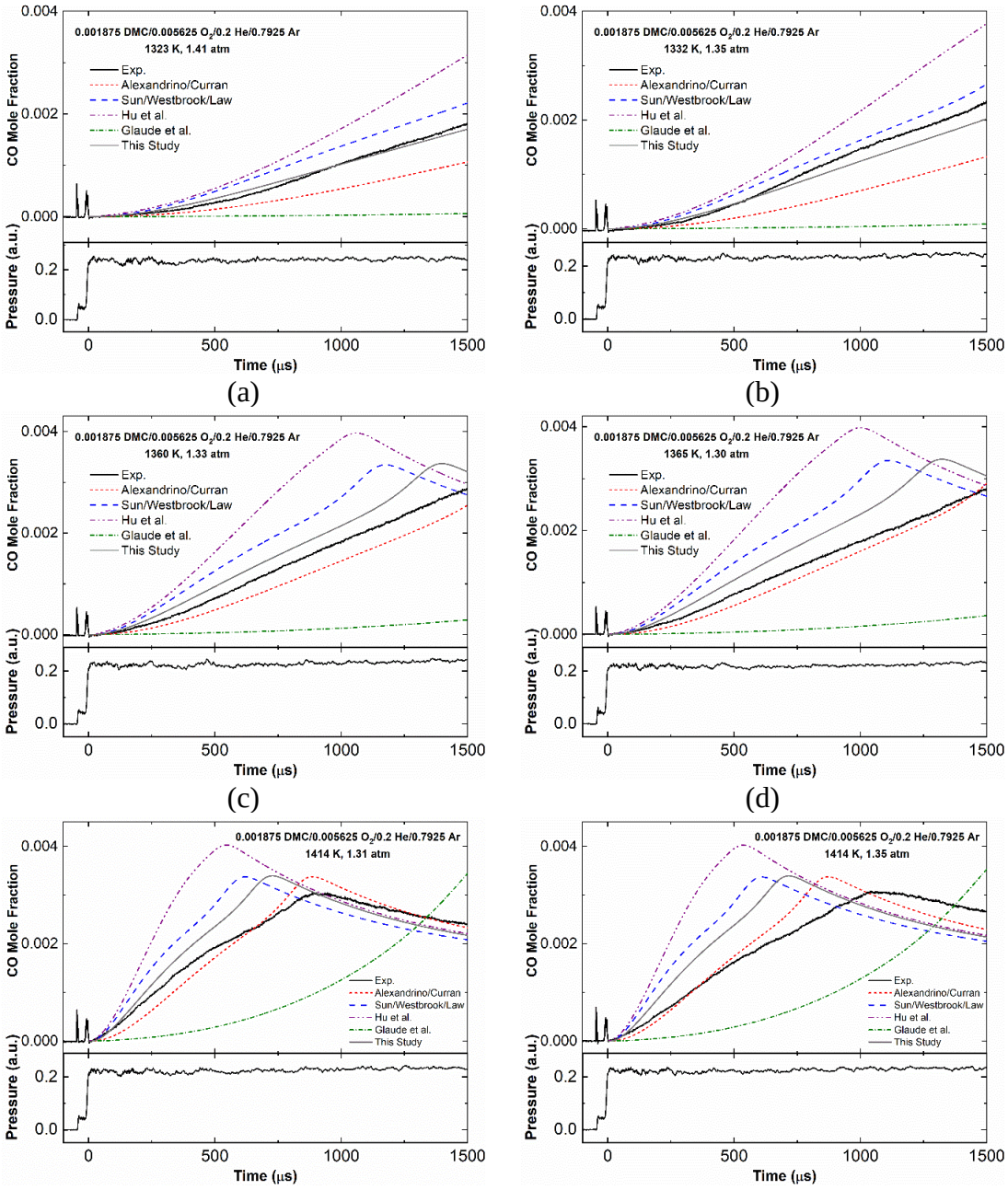

Figure A.4. CO time histories and model comparison for ϕ = 1.0.

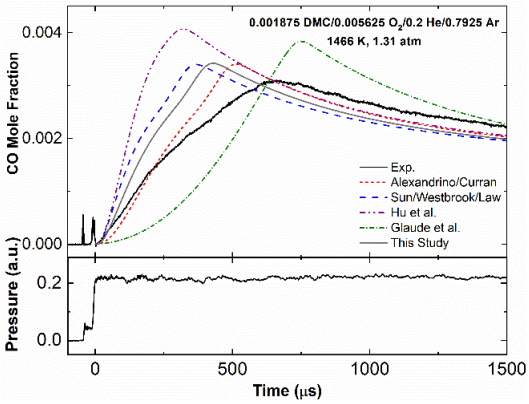

(g)

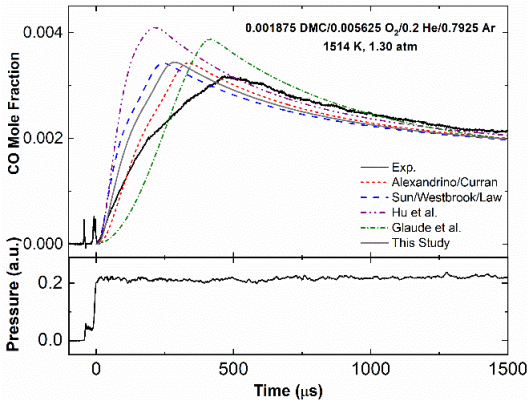

(h)

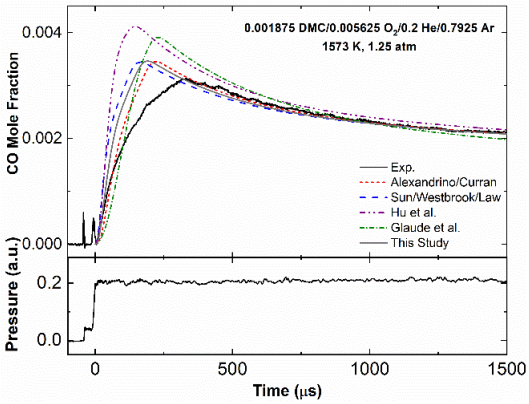

(i)

Figure A.4. CO time histories and model comparison for ϕ = 1.0 – Continued.

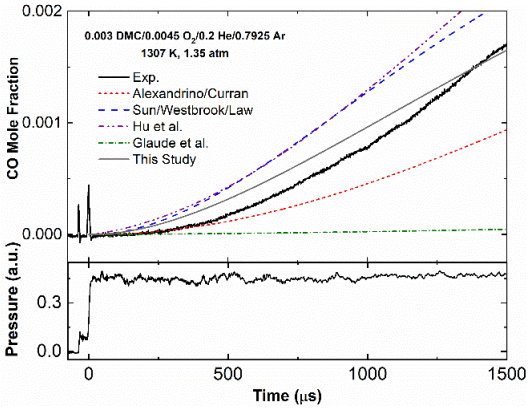

(a)

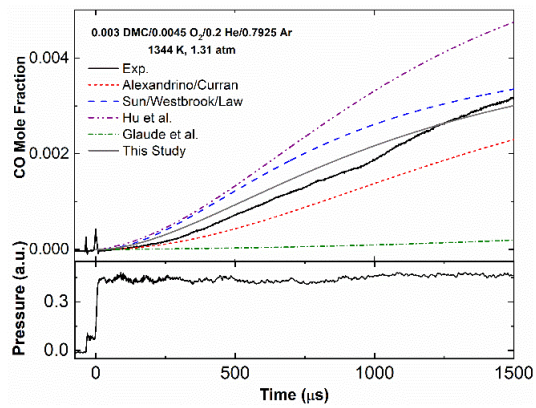

(b)

Figure A.5. CO time histories and model comparison for ϕ = 2.0.

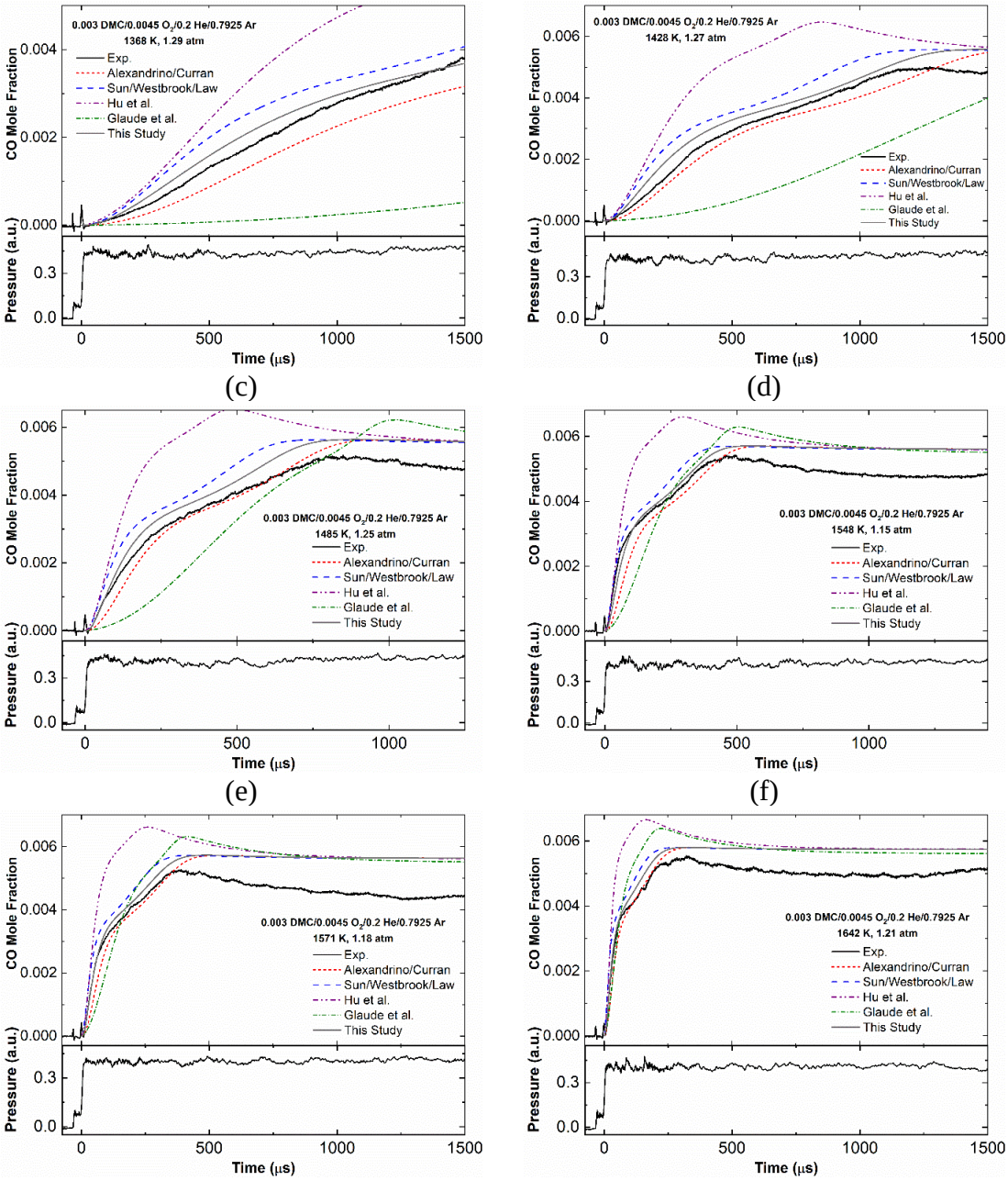

Figure A.5. CO time histories and model comparison for ϕ = 2.0 – Continued.

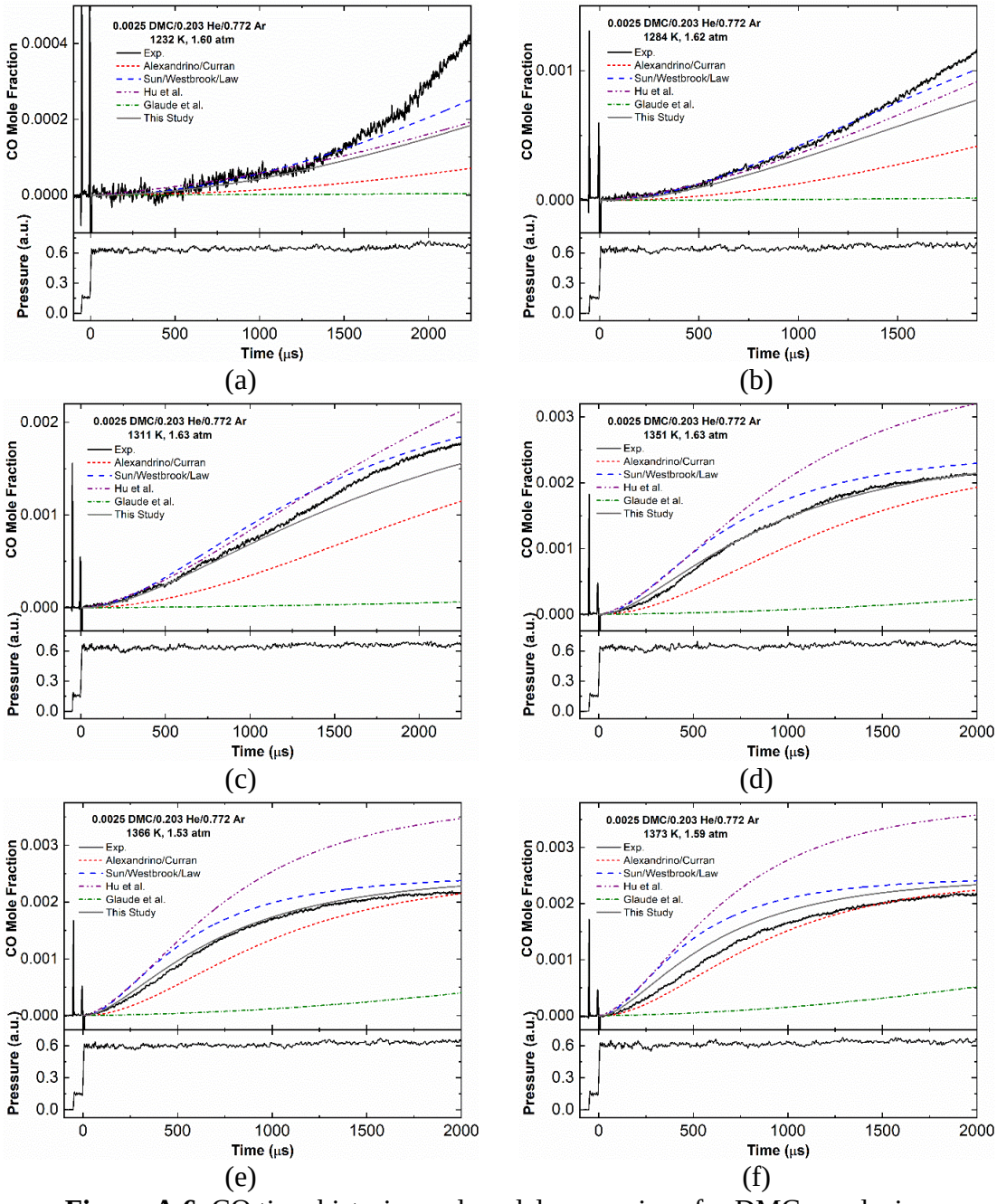

Figure A.6. CO time histories and model comparison for DMC pyrolysis.

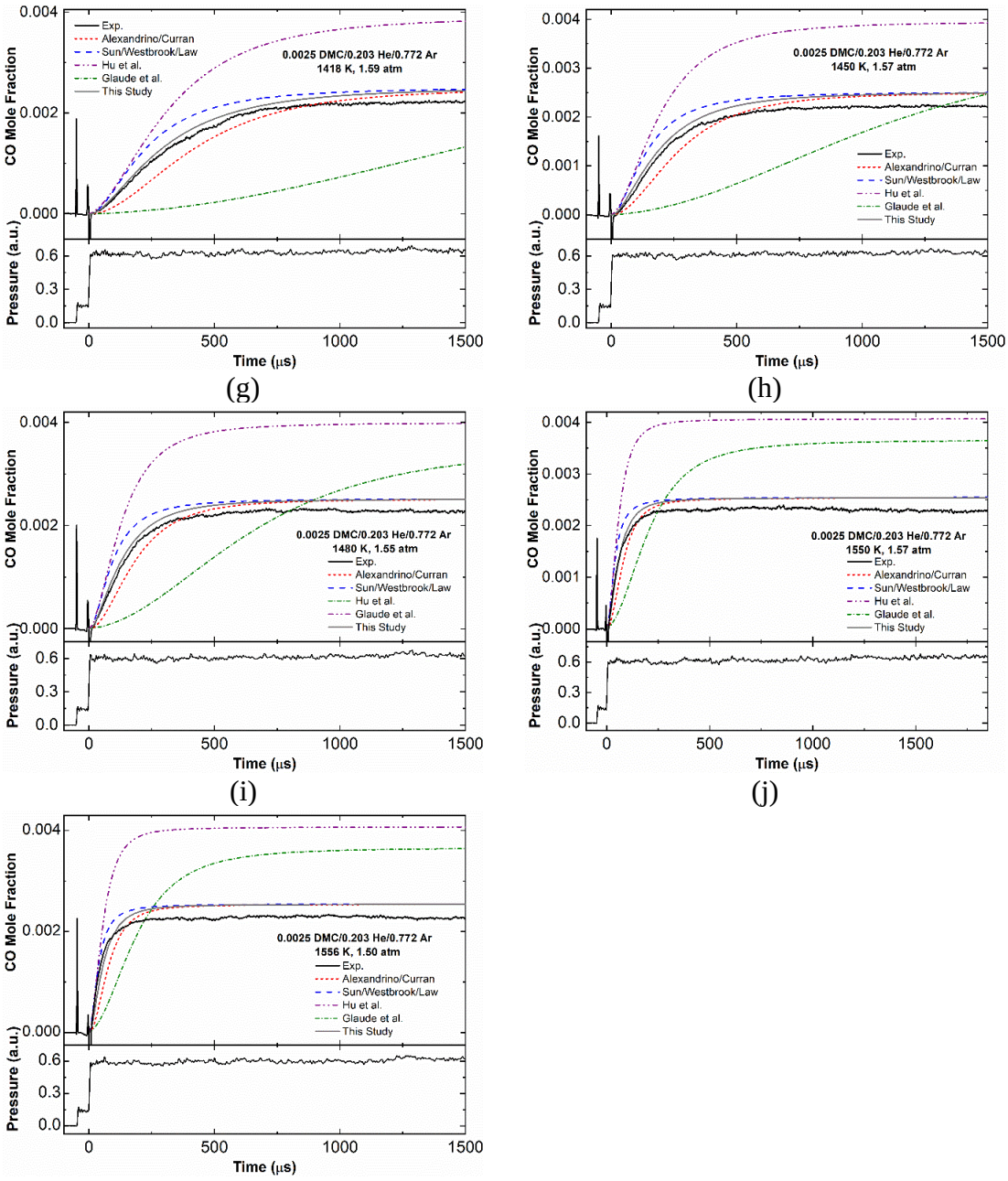

Figure A.6. CO time histories and model comparison for DMC pyrolysis – Continued.

2. H_2O time histories

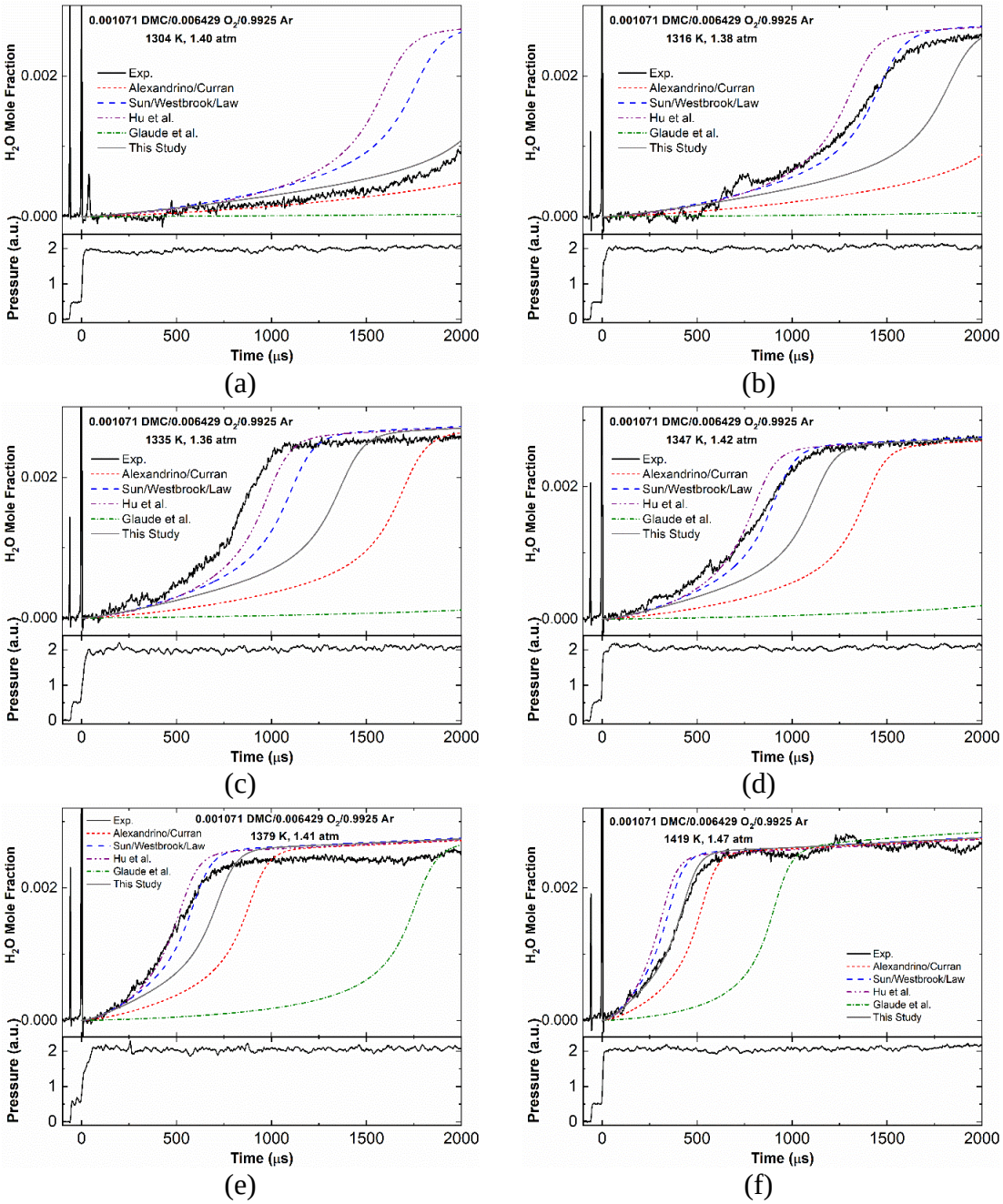

Figure A.7. H_2O time histories and model comparison for $\phi = 0.5$.

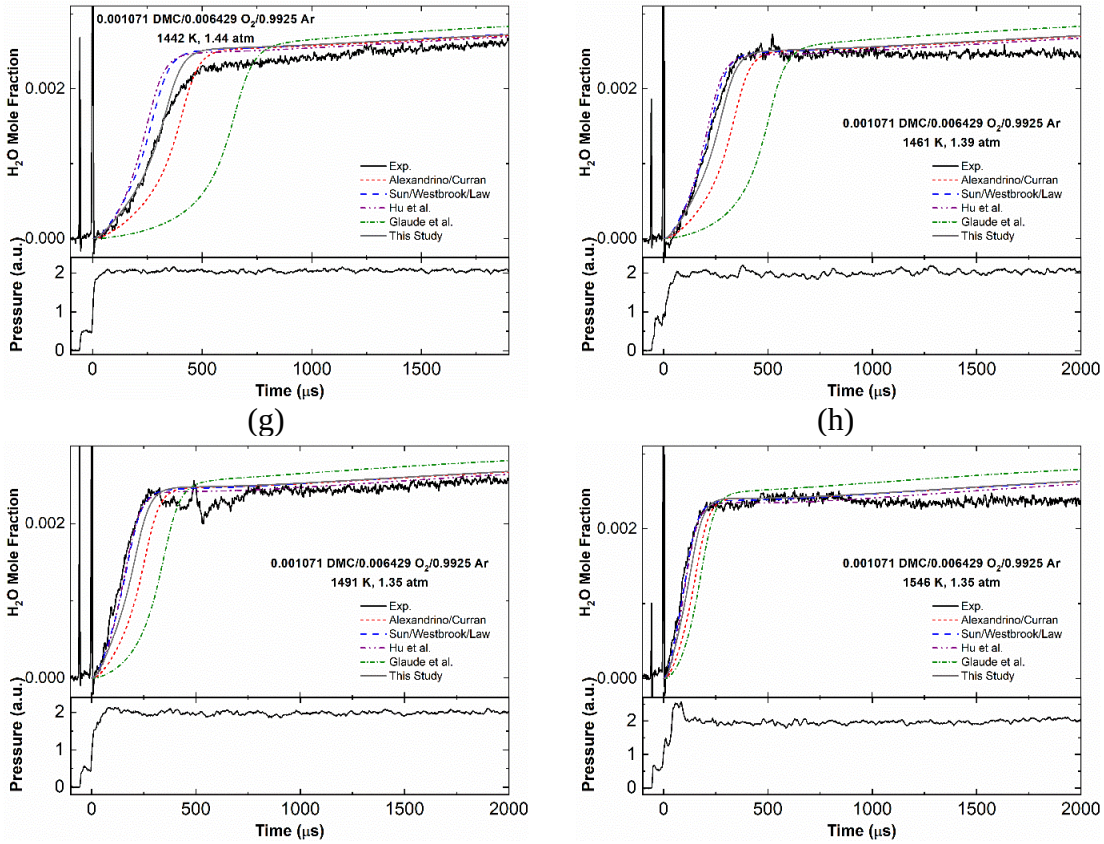

Figure A.7. H_2O time histories and model comparison for ϕ = 0.5 – Continued.

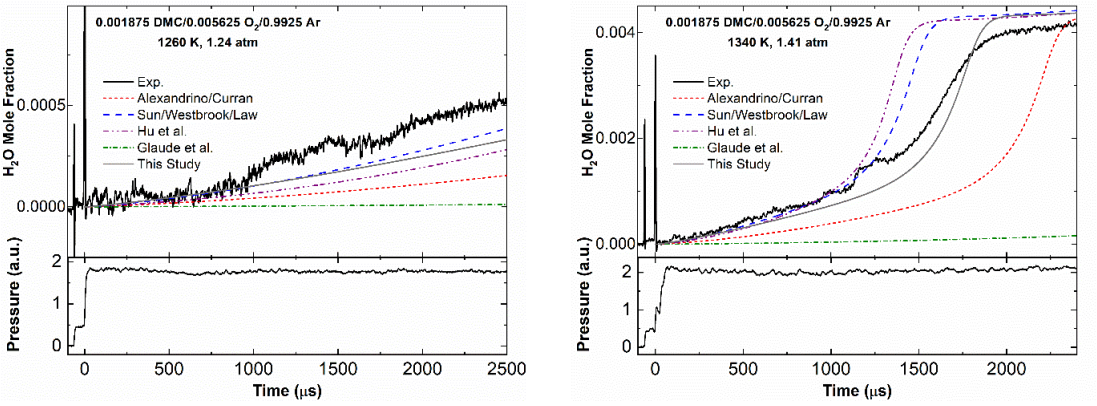

Figure A.8. H_2O time histories and model comparison for ϕ = 1.0.

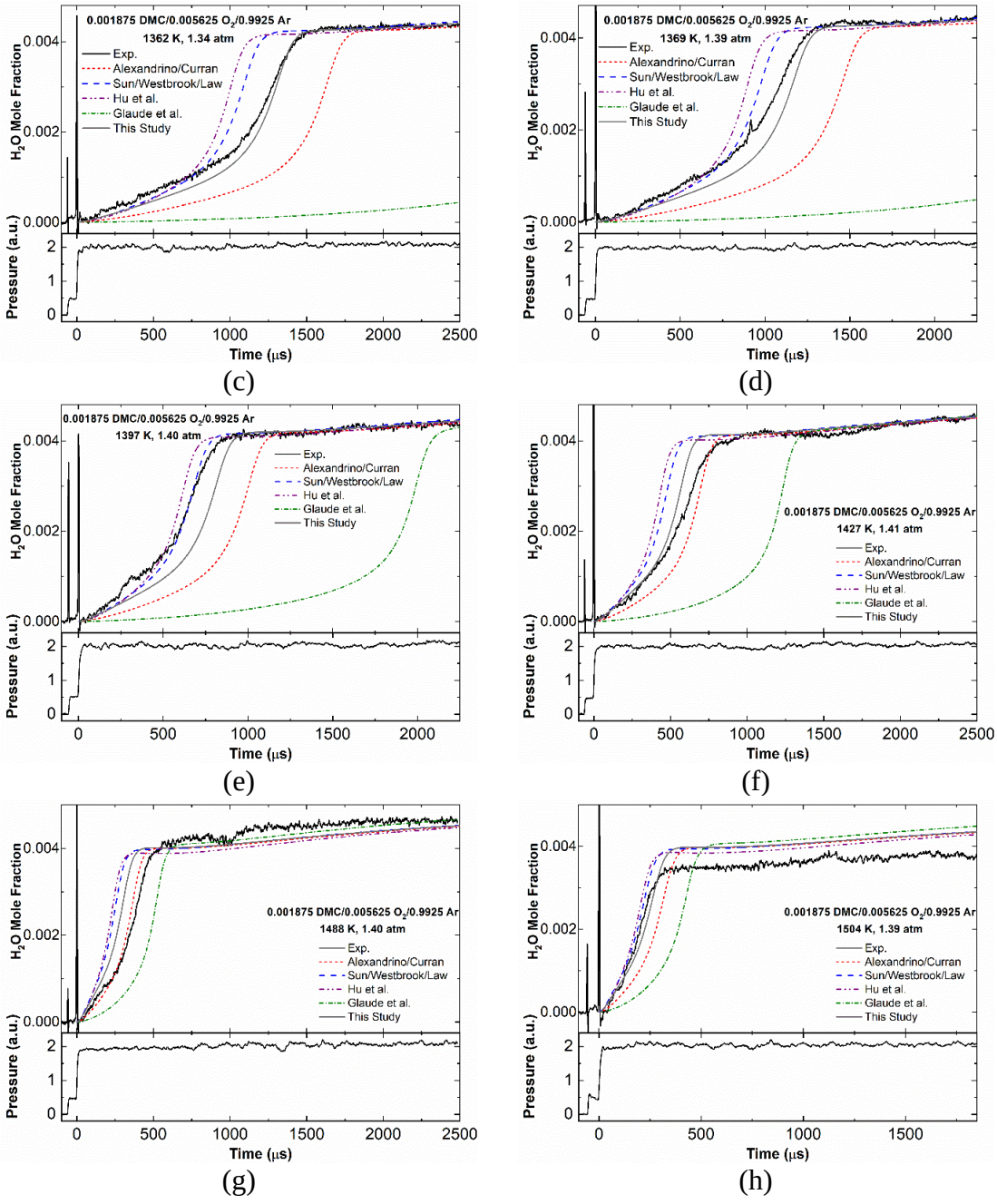

Figure A.8. H_2O time histories and model comparison for $\phi = 1.0$ – Continued.

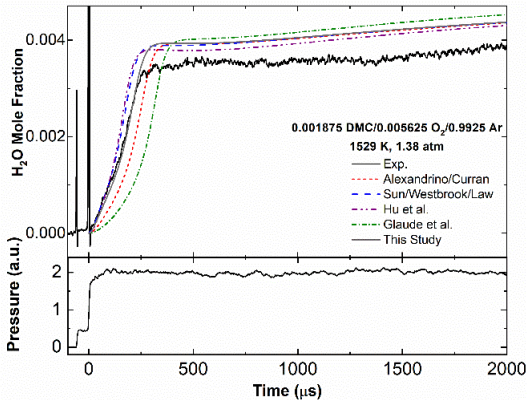

(i)

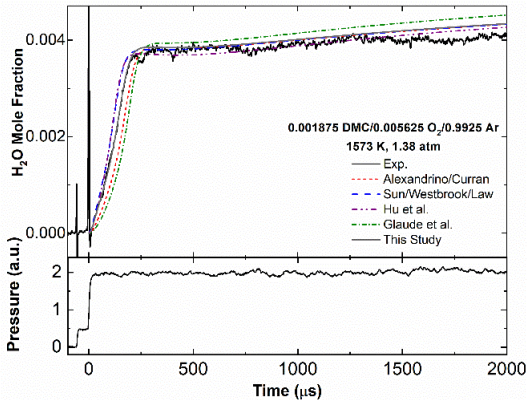

(j)

Figure A.8. H_2O time histories and model comparison for $\phi = 1.0$ – Continued.

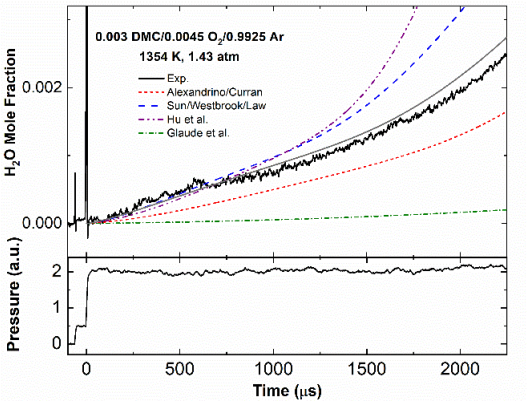

(a)

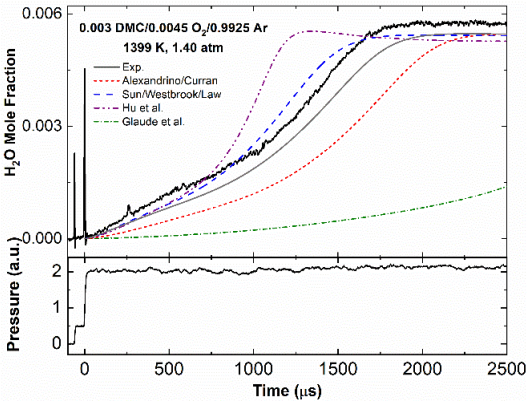

(b)

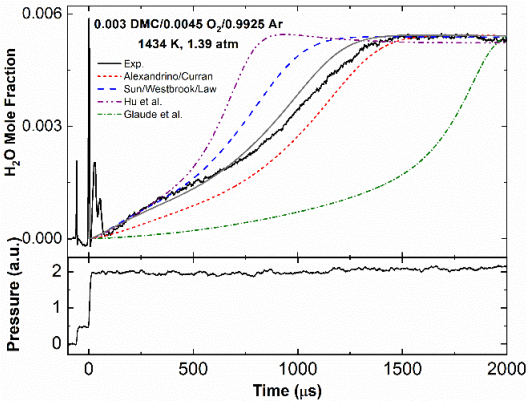

(c)

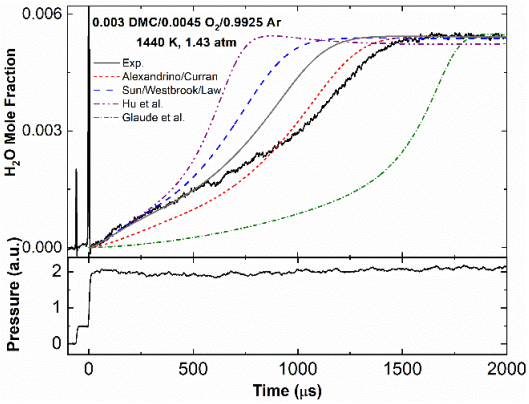

(d)

Figure A.9. H_2O time histories and model comparison for $\phi = 2.0$.

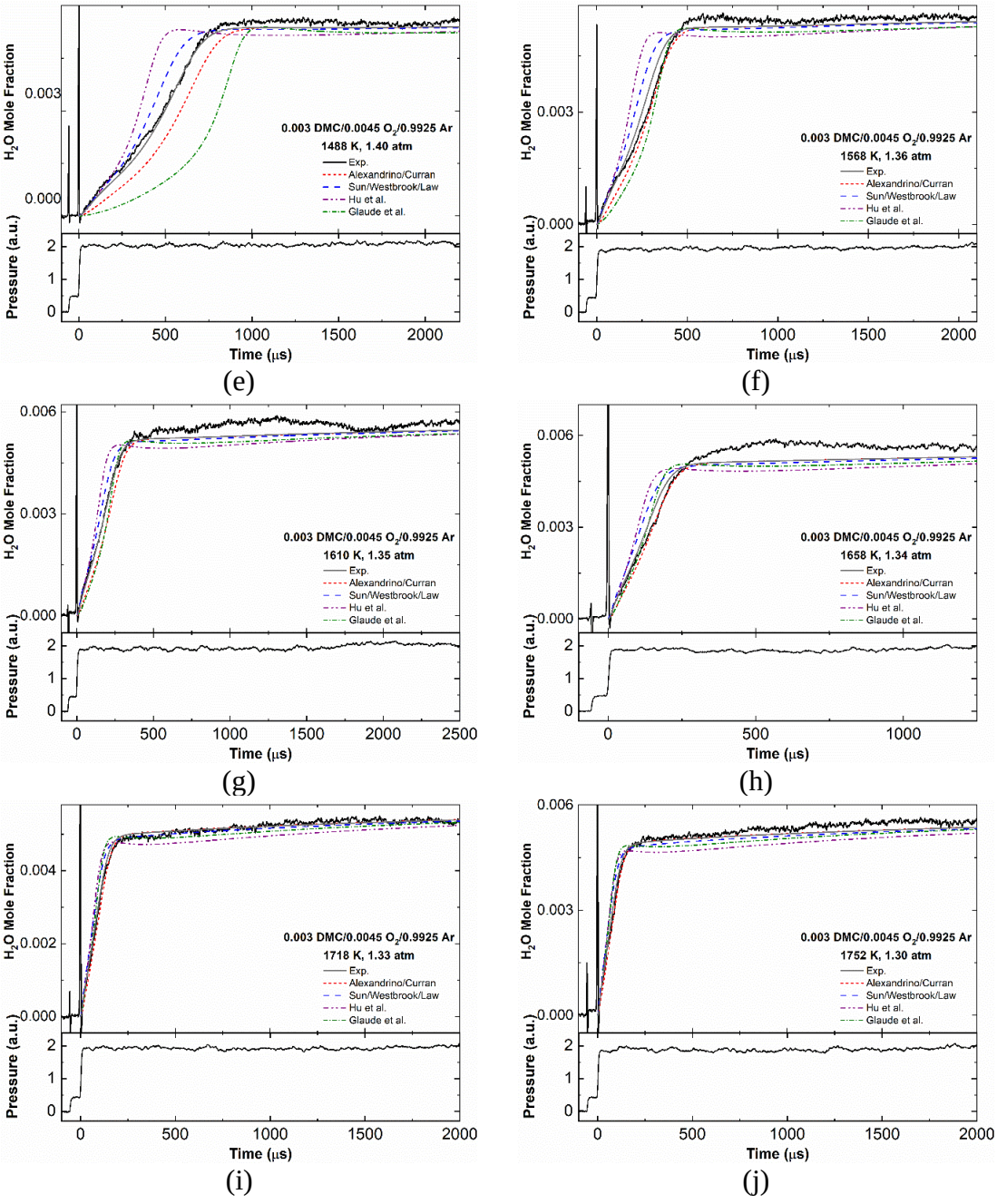

Figure A.9. H_2O time histories and model comparison for $\phi = 2.0$ – Continued.

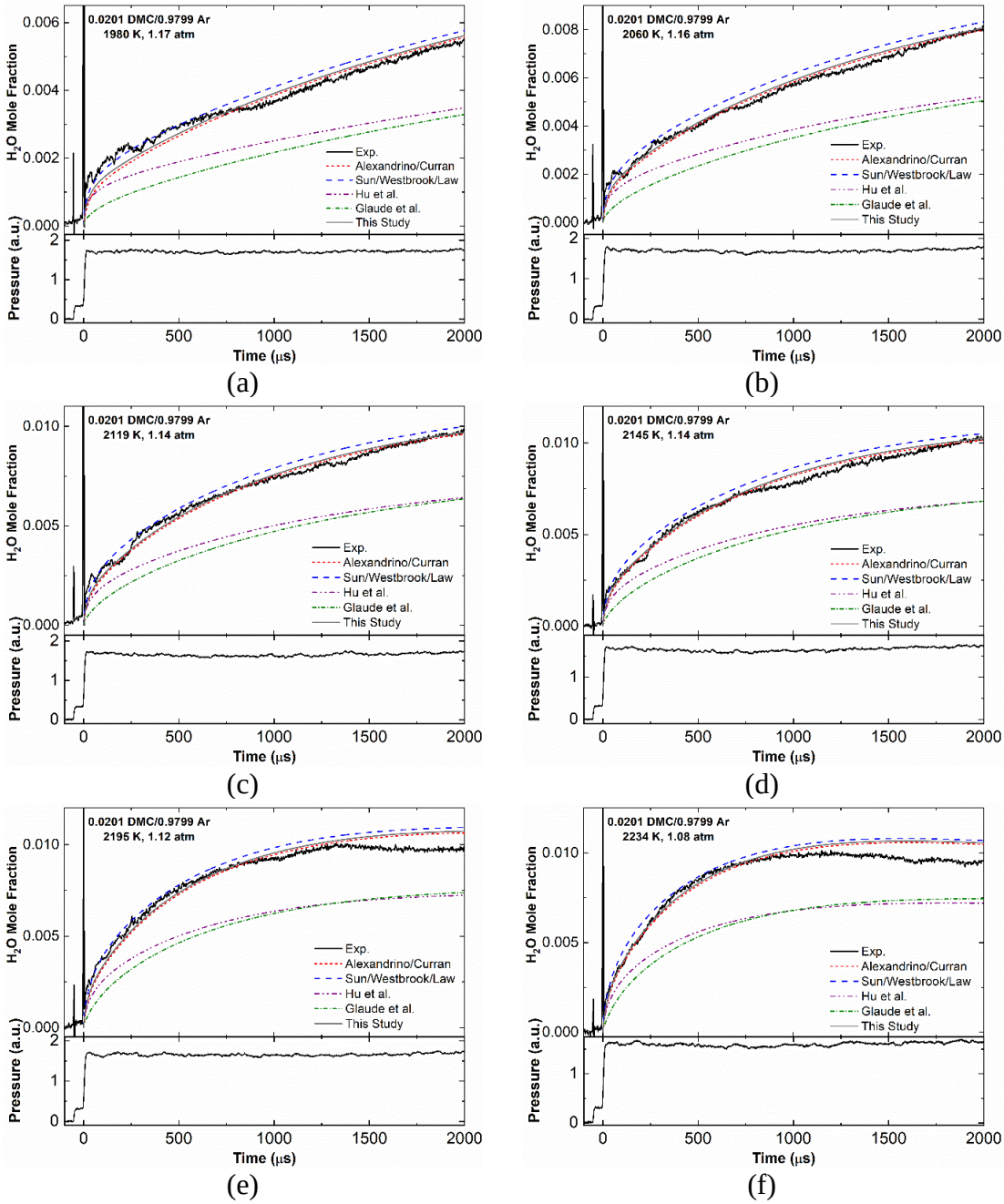

Figure A.10. H_2O time histories and model comparison for DMC pyrolysis (2% in Ar).

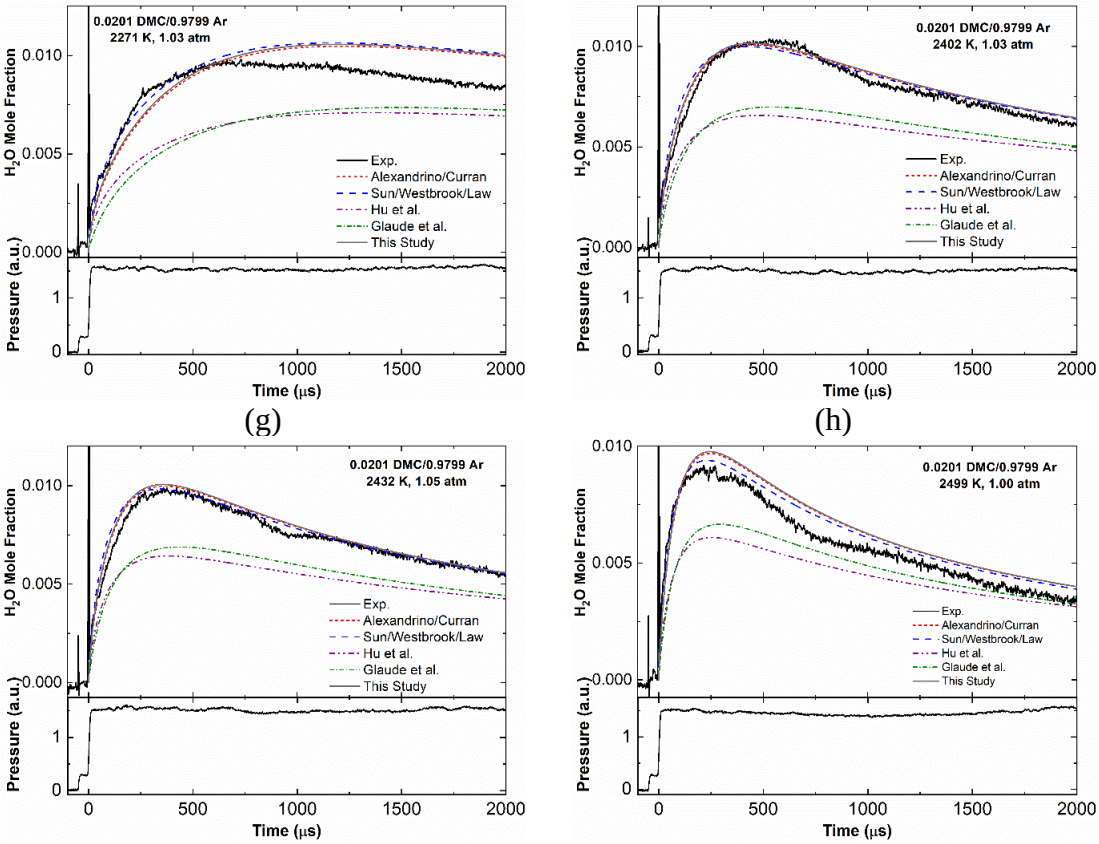

Figure A.10. H_2O time histories and model comparison for DMC pyrolysis (2% in Ar) – Continued.

2. Flame Speed experiments

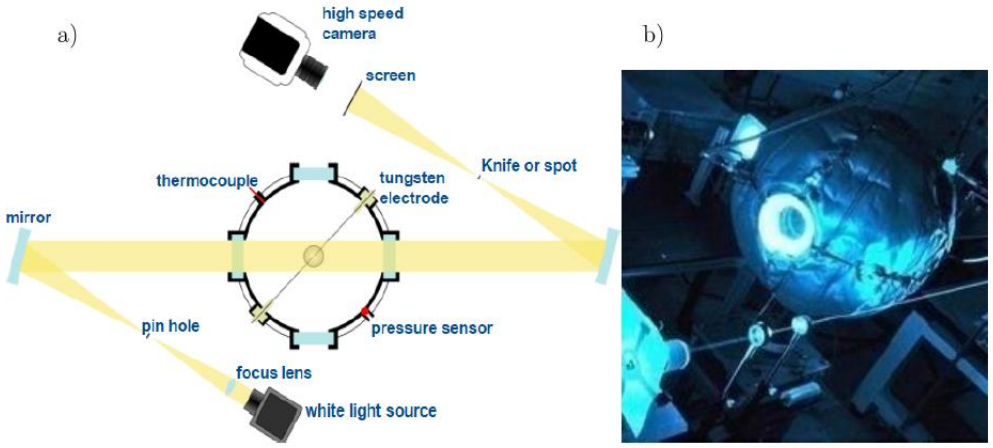

Figure A.11. Flame speed experimental setup. (a) Schematic of the Z-type schlieren, (b) Picture of the flame speed vessel.

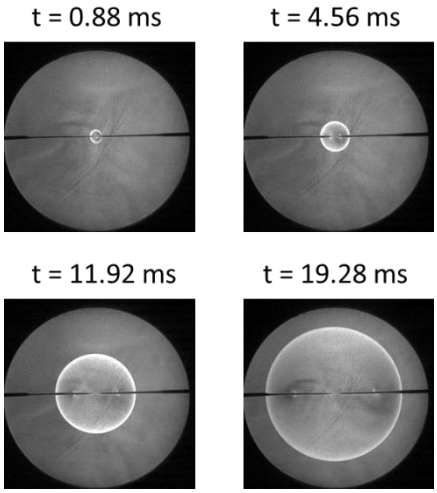

Figure A.12. Typical flame propagation versus time.

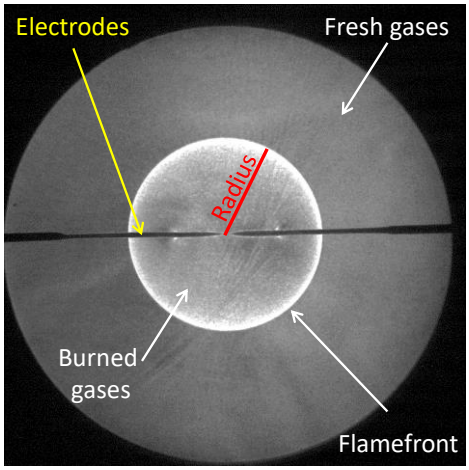

Figure A.13. Typical view of a Matlab processed image.

3. Tentative Model Sensitivity Analysis

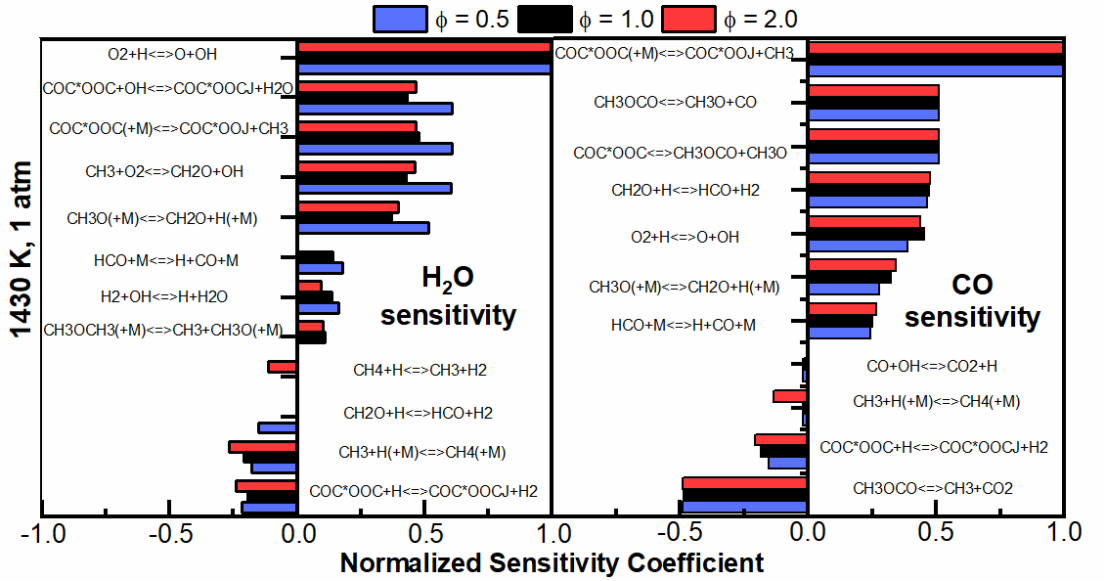

Figure A.14. Sensitivity analysis at intermediate temperature using tentative model.

4. Khaled et al. reaction rates and model comparisons

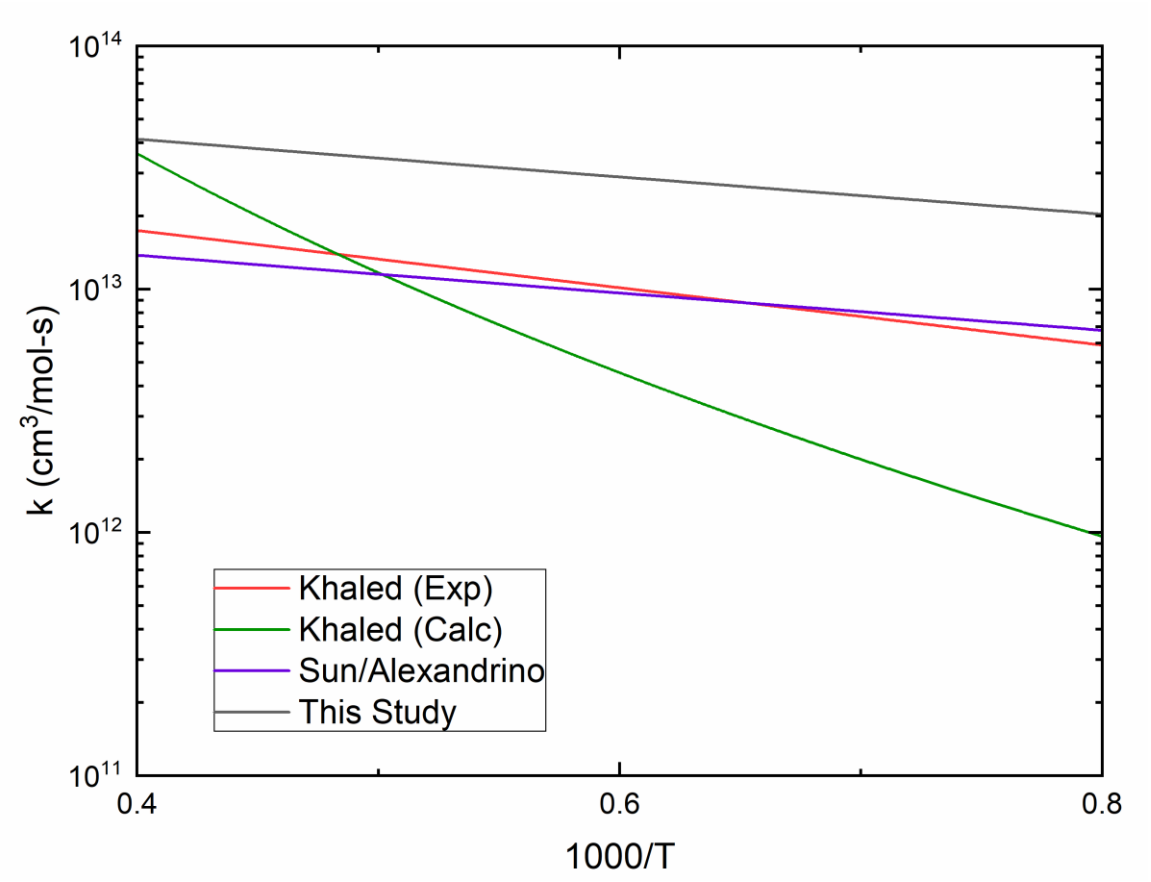

Figure A.15. DMC + OH reaction rates comparison.

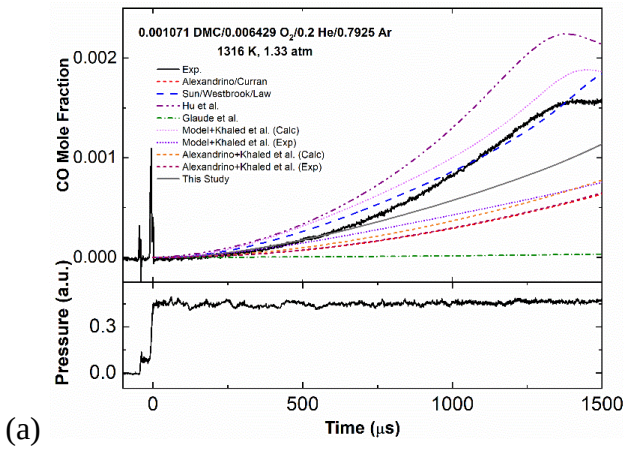

(a)

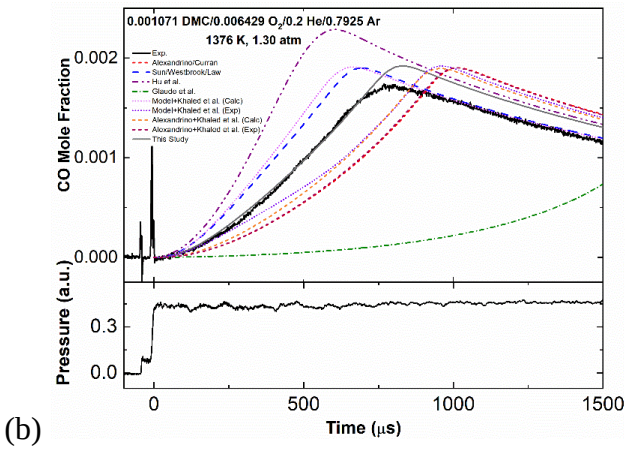

(b)

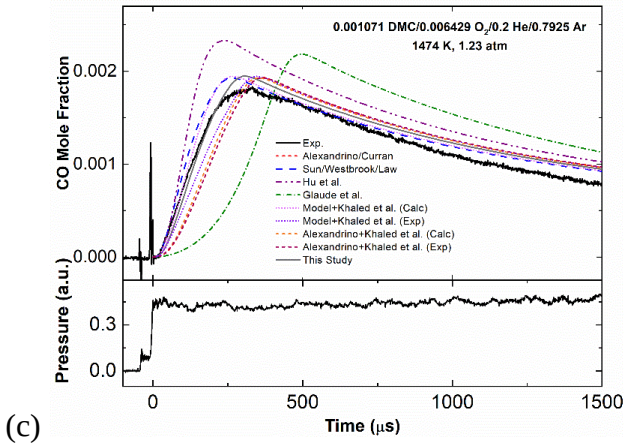

(c)

Figure A.16. CO time histories and model comparison for phi 0.5 at (a) low-, (b) mid- and (c) high-temperatures. Note: "Model+…" refers to the tentative model using Khaled et al. rates.

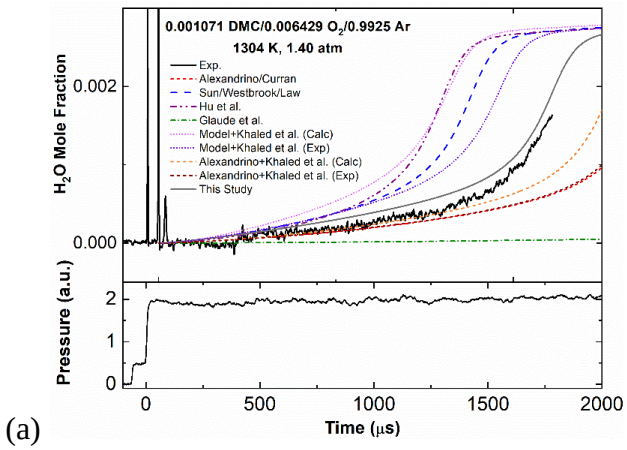

(a)

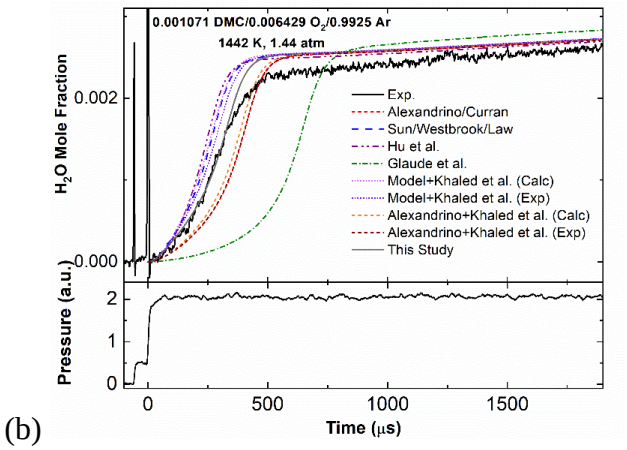

(b)

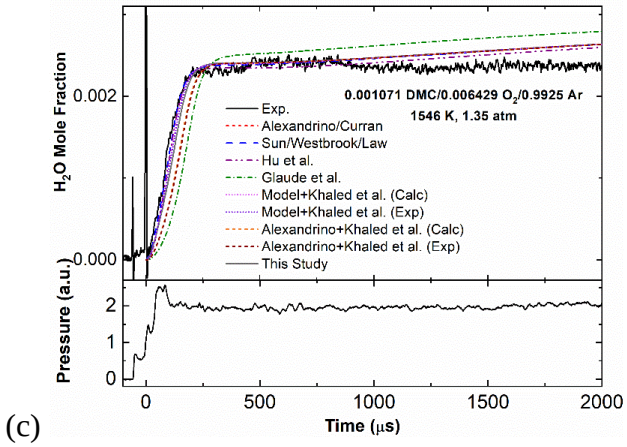

(c)

Figure A.17. H_2O time histories and model comparison for phi 0.5 at (a) low-, (b) mid- and (c) high-temperatures. Note: "Model+…" refers to the tentative model using Khaled et al. rates.